

A review on perovskite solar cells: Evolution of architecture, fabrication techniques, commercialization issues and status



Priyanka Roy^a, Numeshwar Kumar Sinha^a, Sanjay Tiwari^b, Ayush Khare^a

^a Thin Film Research Laboratory, Department of Physics, National Institute of Technology, G E Road, Raipur 492 010, India

^b School of Studies in Electronics and Photonics, Pt. Ravishankar Shukla University, Raipur 492 010, India

ARTICLE INFO

Keywords:

Perovskite
Cell architecture
Fabrication
Toxicity
Degradation
Commercialization

ABSTRACT

Perovskite Solar Cells (PSCs) have grabbed the attention of the researchers worldwide owing to their outstanding Photovoltaic (PV) performance. PSCs are the future of the PV technology as they are capable of generating power with performance being comparable with the leading Silicon solar cells, with the cost being lower than Silicon solar cells. The enormous potential of PSCs is evident from the fact that the efficiency of these cells has risen from 3.8% to 25.2% within a decade, and it is continuously rising to date. We discuss the features making PSCs superior to contemporary PV technologies. The description of the evolution of efficiency and various architectures used to date has been presented. The perovskite film fabrication techniques with some large scale perovskite solar cell manufacturing techniques are discussed. Despite positive traits, the PSCs have faced some issues, such as degradation in the presence of moisture, oxygen, and UV, toxicity, etc. The impact of these factors with various remedies adopted by researchers has been discussed. However, the instability issue raised by toxicity is not of much concern is supported in this paper. These issues creating obstacles in the path of commercialization of PSCs along with the commercialization road map are discussed thoroughly.

1. Introduction

For last so many years, the mankind has been looking for a source of energy that is not only environmentally sustainable but is commercially viable as well. Current global power demand is about 16TW, and it is estimated that the power demand would increase beyond 30TW by 2050. Therefore, rigorous research is being carried out to get an efficient power generation system, as the traditional technique of burning fossil fuel would not be able to meet the hike in the power requirement. The renewable energy sources, such as tidal, hydrothermal, geothermal, wind, solar, etc. will act as a savior in the energy crises. Among the various sources of energy, solar energy is believed to be the most promising and efficient one due to its availability in abundance. The uniqueness of solar energy can also be inferred from the fact that one hour of continuous illumination of solar energy is capable of fulfilling our annual power demands, if all the incident solar energy is converted into electricity. So, using PV solar cells for power generation seems to be a promising way as they convert the sunlight directly into electricity.

In 1839, Edmund Becquerel was the first to convert sunlight into electricity. In 1873, Willoughby Smith discovered photoconductivity (PC) in selenium. In 1883, Charles Fritts proposed the first design of PV cell, which was based on the Selenium wafers. The theory of photoelectric effect proposed by Albert Einstein in 1905 explained how light

knocks out the electron from the metal surface. Later for this work, he was awarded with the Nobel Prize. In 1918, Jan Czochralski laid the foundation of Silicon (Si) based solar cells by developing a technique to grow single-crystal silicon (Si) ([The History of Solar Energy, 2013](#)). In 1954, the birth of PV occurred, when the crystalline silicon-based solar cell was developed in Bell lab, USA that had power conversion efficiency (PCE) of 4.5% ([Chapin et al., 1954](#)). Since then, researchers have been actively searching for a low-cost device structure and some new materials exhibiting the PV effect. As a result, second-generation solar cells came into existence. These cells were basically based upon III-V device structure, GaAs, CdTe, InP, and CIGs solar cells were introduced in the field of solar photovoltaics ([Green et al., 2018](#)). The early 1990s came up with the third generation of solar cells with Dye-sensitized structure. In 2000s Organic Photovoltaic cells (OPV) were introduced. With growing interest in nanomaterials, intensive research work is being carried out for finding new materials in the field of solar devices, which are not only cheap but requires low-cost processing conditions as well. Currently, crystalline silicon solar cells dominate the market, but the factors, such as the requirement of the expensive manufacturing process and costly raw materials are urging researchers to come up with a new PV technology that has the combination of both high efficiency and low-cost manufacturing. The perovskite materials are gaining huge interest among the researchers because of their brilliant PV

E-mail address: akhare.phy@nitrr.ac.in (A. Khare).

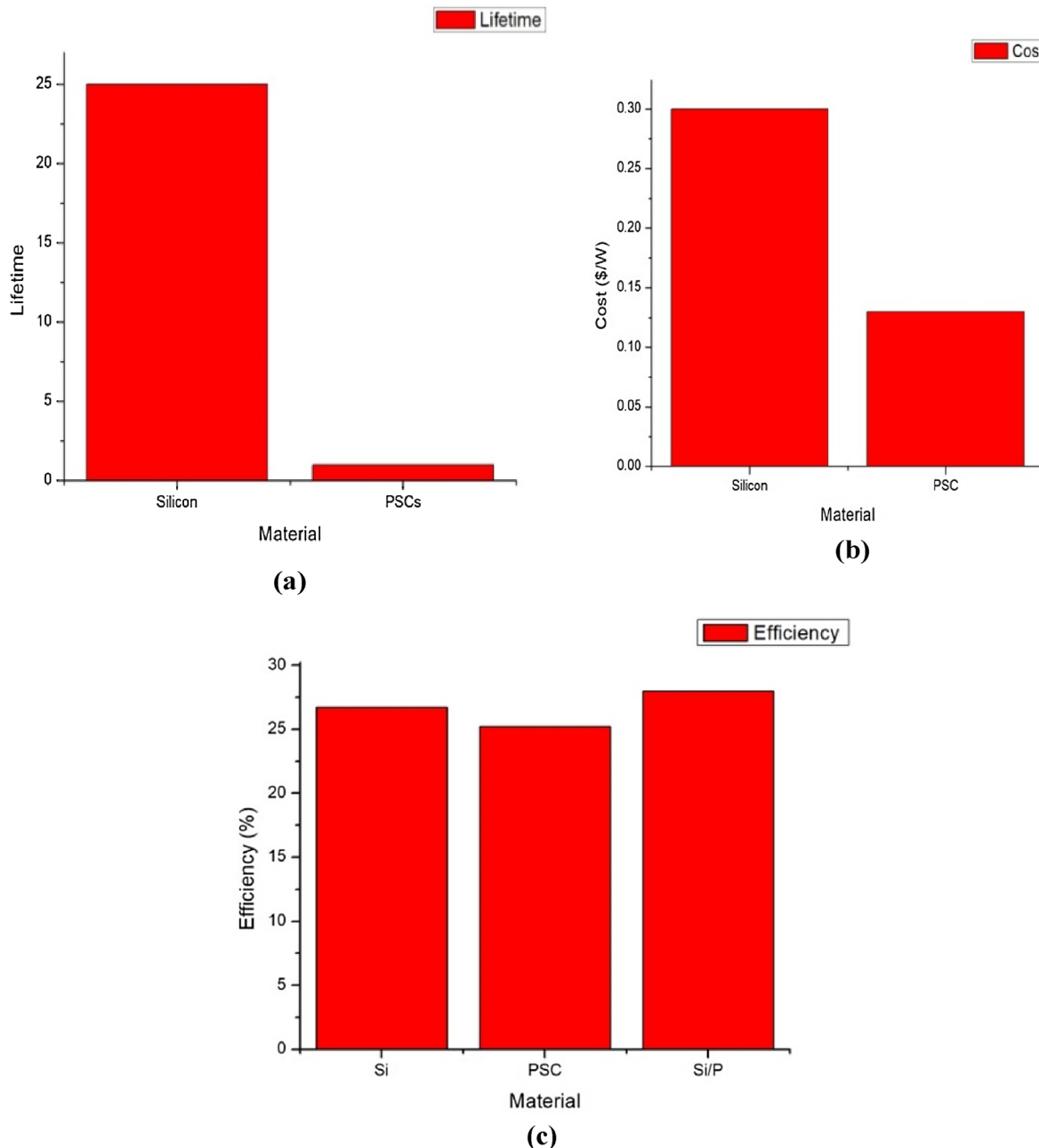


Fig. 1. Comparison of performance of PSC and Silicon solar cell (a) comparison of cost (b) comparison of lifetime (c) comparison of efficiency of silicon, PSC and Si/P tandem cell.

performance, low-cost raw material, and requirement of easy processing conditions (Zhou et al., 2018). The PSCs do not require any sophisticated processing conditions; instead, they can be synthesized in laboratories using wet chemistry with the help of simple low-cost techniques, such as spin coating, dip coating, screen printing, dual source evaporation techniques, etc. The perovskite materials can also be grown on a flexible substrate. Despite all the merits, poor device stability and short lifetime are creating hindrances in the path of commercialization of PSCs. In this review, we present the historical background of PSCs, a brief discussion in the evolution of the device architecture, fabrication techniques, degradation causing factors and present commercialization status. The enormous capability of PSCs is evident from the abrupt increment in the power conversion efficiency (PCE) from 3% to 25.2% (28% in tandem architecture) over the past 10 years (Kojima et al., 2009; Best Research-Cell, 2019) while other technologies took nearly 30 years to witness this milestone. Perovskites

material incorporated in a solar cell can serve as both, an absorber layer and an efficient charge transport layer (Mei et al., 2014). The performance comparison of PSC and Silicon solar cell is illustrated in Fig. 1.

The perovskite materials are considered as one of the eminent materials for new generation PV technology because of their unique properties, such as high electron mobility ($800 \text{ cm}^2/\text{Vs}$) (Valverde-Chávez et al., 2015), high carrier diffusion length (exceeding $1 \mu\text{m}$) (Miyata et al., 2015; Xing et al., 2013), ambipolar charge transport behaviour (Information, 2013), high absorption coefficient (greater than 10^5 cm^{-1}) due to s-p antibonding coupling, low exciton binding energy (less than 10 meV) (Miyata et al., 2015), high photoluminescence (PL) quantum efficiency (as high as 70%), high carrier lifetime (exceeding 300 ns), optimum bandgap, low surface recombination velocity, tunable bandgap, great structural defect tolerance, and amiable grain boundary effect. The main difference between inorganic and organic absorbers is in the exciton type. The organic absorber layer has

Table 1
Properties of perovskite materials.

Properties	Value Range
Bandgap	1.5–2.5 eV
Absorption coefficient	10^5 cm^{-1}
Exciton binding energy	Less than 10 meV
Crystallization energy barrier	$56.6\text{--}97.3 \text{ kJ mol}^{-1}$
PL quantum efficiency	70%
Charge carrier lifetime	Greater than 300 nm
Relative permittivity	3
Carrier mobility	$800 \text{ cm}^2/\text{Vs}$
Exciton	Wannier type
Trap-state density	10^{10} cm^{-3} (single crystals), $10^{15}\text{--}10^{17} \text{ cm}^{-3}$ (polycrystalline)

basically Frenkel type exciton while the inorganic layer has Wannier type. The perovskite material used in solar cells has Wannier type exciton. Therefore, the generated charge carriers behave in the same manner as they do in inorganic material (Hirayama et al., 1994; Minemoto and Murata, 2014). The properties of perovskite materials are summarized in the Table 1 and the PCE of various cells to date is shown in Table 2. The properties indeed are adjustable by controlling the shape and size of the constituent particles during fabrication.

2. History of perovskite solar cells

The perovskite is basically Calcium titanium oxide (CaTiO_3). It is a mineral found by Gustav Rose in the Ural Mountains of Russia in 1939. Count Lev Alekseevich Perovski (1972–1856), a Russian mineralogist further carried the research and thus, the material was named after him as ‘Perovskite’ (Miyata et al., 2015). In the 1990s, Mitzi and co-workers investigated the optoelectronic properties of the organic-inorganic perovskites. They reported that the material exhibited strong exciton features, and further suggested that it could be used in the field of LEDs, transistors and solar cells (Mitzi et al., 2010; Chess et al., 2006). The phenomenon of PV generation was first seen in this material by Kojima and coworkers. In 2009, they were first to use perovskite material in solar cells by utilizing it as a liquid sensitizer in DSSC configuration. The MAPbI_3 and MAPbBr_3 (where MA stands for CH_3NH_3) were used as

liquid sensitizers, and the device attained an efficiency of 3.81% and 3.2%, respectively. However, the device was highly unstable and lasted only for a few seconds due to the presence of liquid electrolyte (Kojima et al., 2009). Park et al. used quantum dots of nanocrystalline material and utilized similar dye-sensitized concepts. They raised the cell efficiency from 3.8% to 6.54%, but the device collapsed after 10 min of successful operation due to the dissolution of MAPbI_3 quantum dots into the redox electrolyte solution (Im et al., 2011). Because of the instability raised due to the presence of liquid electrolytes, this configuration did not gain much attention. In 2012, Kim et al. overcame the problem arising due to the presence of liquid electrolytes by fabricating an all-solid-state PSC. The Spiro-OMeTAD was used as a hole transport layer and the device attained an efficiency of 9.7%. This made a remarkable change in the history of the perovskite sensitized solar cells as it not only raised the efficiency but also made a considerable enhancement in the lifetime by withstanding ex-situ long term stability test for about 500 h without any encapsulation (Kim et al., 2012). In 2013, Burschka et al. obtained an efficiency of 15% by using the 2-step sequential deposition technique, and fabricated the cell in planar architecture. They adopted the sequential deposition technique where they first deposited PbI_2 layer followed by deposition of $\text{CH}_3\text{NH}_3\text{I}$ instead of processing both of them together. This structure gave a high J_{sc} (20 mA/cm^2) due to the creation of a dense and uniform perovskite layer (Burschka et al., 2013). In 2014, Im et al. fabricated MAPbI_3 based solar cells using two-step solution processing. They attained a high performance by controlling the size of MAPbI_3 cuboid, which enabled proper light-harvesting and enhanced charge transportation. They reported that the cuboid size depended on the concentration of MAI solution and also upon the exposure time of PbI_2 to MAI before spin coating. This group of researchers obtained an improved PSC with an efficiency of 17.01% (Im et al., 2014). Giordano et al. in 2015, improved the electronic properties of mesoporous titania layer (m-TiO_2) by the addition of Lithium (Li) in it and attained superior device performance with PCE of 19.3%. The Li doped mesoporous titania layer (m-TiO_2) gave better electronic properties and faster electronic transportation due to the reduction in electronic trap states. This device exhibited negligible hysteresis loss (less than 0.3%) (Giordano et al., 2016). In 2015, Yang et al. demonstrated a technique to deposit

Table 2
The PCE of various PV cells to date.

Solar cell	Types	Efficiency	Developer name
Silicon	Single crystal	26.1 (NREL. PV Research Cell Record Efficiency Chart, 2019)	ISFH (Institute for Solar Energy Research Hamelin)
	Poly-cry	22.3 (NREL. PV Research Cell Record Efficiency Chart, 2019)	FhG-ISE (Fraunhofer Institute for Solar Energy Systems)
	Thin film	21.2 (NREL. PV Research Cell Record Efficiency Chart, 2019)	Solexel
	a-Si: H	14 (NREL. PV Research Cell Record Efficiency Chart, 2019)	AIST (National Institute of Advanced Industrial Science and Technology)
	Silicon hetero-structure	26.7 (NREL. PV Research Cell Record Efficiency Chart, 2019)	Kaneka (Kaneka Solar Energy)
GaAs	Single crystal	27.8 (NREL. PV Research Cell Record Efficiency Chart, 2019)	LG (LG Electronics)
	Thin-film	29.1 (NREL. PV Research Cell Record Efficiency Chart, 2019)	Alta device
CIGS		23.4 (NREL. PV Research Cell Record Efficiency Chart, 2019)	SolarFron (Solar Frontier)
CdTe		22.1 (NREL. PV Research Cell Record Efficiency Chart, 2019)	FirstSolar (First Solar Inc)
Quantum dot		16.6 (NREL. PV Research Cell Record Efficiency Chart, 2019)	Univ. Of Queensland
Dye-sensitized		11.9 (NREL. PV Research Cell Record Efficiency Chart, 2019)	Sharp (Sharp Solar)
Organic		16.5 (NREL. PV Research Cell Record Efficiency Chart, 2019)	SCUT-CSU (South China University of Technology - Central South University)
Perovskite		25.2 (NREL. PV Research Cell Record Efficiency Chart, 2019)	KRICT/MIT (Korea Research Institute of Chemical Technology/ Massachusetts Institute of Technology)

improved quality FAPbI₃ film with (1 1 1) crystallographic orientation, uniform, dense and large microstructures. They used FAPbI₃ instead of MAPbI₃ and attained power conversion efficiency (PCE) of 20.2% (Yang et al., 2015). In 2016, Li et al. fabricated a perovskite film with uniform morphology and crystalline behavior by using the vacuum flash solution processing method (VASP). They used FA_{0.81}MA_{0.15}PbI_{2.51}Br_{0.45} as an absorber layer and attained PCE of 20.5% (Li et al., 2016). In 2016, Bi et al. introduced a new approach for perovskite film fabrication and attained improved electronic property by using a polymer. They improved the growth and nucleation processes by using poly (methyl methacrylate) (PMMA) and attained PCE of 21.6% (Bi et al., 2016). Recently, Yang et al. used multiple cations (comprising FA) and mixed halide anion as an absorber layer. They succeeded in reducing the concentration of deep-level defect states by the addition of iodide solution into the organic cation solution. This defect engineering enabled the scientists to achieve an efficiency of 22.1% for small scale and 19.7% in 1 cm² cell (Yang et al., 2017). Then came the breakthrough in 2018 when researchers from Chinese Academy of Sciences attained the highest efficiency of 23.3%. Further, in December last year, the maximum efficiency of single-junction silicon solar cell was defeated by Perovskite in tandem architecture along with Silicon by attaining PCE of 28% (Oxford, 2018). The efficiency of single-junction PSC was raised to 23.7% and high V_{oc} closer to the bandgap was attained by tailoring a high quality perovskite layer offereing minimum recombination loss (Kim et al., 2019). Currently, the highest efficiency of single-junction PSC has reached 25.2% by KRICT (South Korea) (NREL Efficiency Chart, 2019). They used a highly efficient hole conductor layer, Nickel oxide (NiO_x), which is deposited over a large area. NiO_x is an inexpensive material and it has ability to withstand high temperatures up to 70 °C. The layers were deposited by rotatory coating method (Highly efficient solar cells thanks to solid foundation, 2019). The advancement in the progress of PSCs in past years is shown in Fig. 2. It is seen that, as compared to silicon solar cells the PSCs exhibit rapid development. The details of PSCs are enclosed in Table 3.

It is important to note that all the leading perovskite solar cells (PSCs) have the incorporation of Formamidinium (FA) as cation which is also believed to be more stable than Methylammonium (MA) and also has an optimal red-shifted bandgap. However, the size of FA is very large, which produces lattice distortion (Eperon et al., 2014; Jeon et al., 2015). Now the power conversion efficiency (PCE) of perovskite-based solar cells is expected to reach up to 30% by 2020. Apart from the extensive research going in efficiency hike, work is also being done to increase the stability and lifetime of perovskite solar cells (PSC). Gracini et al. engineered an ultra-stable 3D/2D CH₃NH₃PbI₃ perovskite junction that had PCE of 13% and was stable for one year (Gracini et al., 2017).

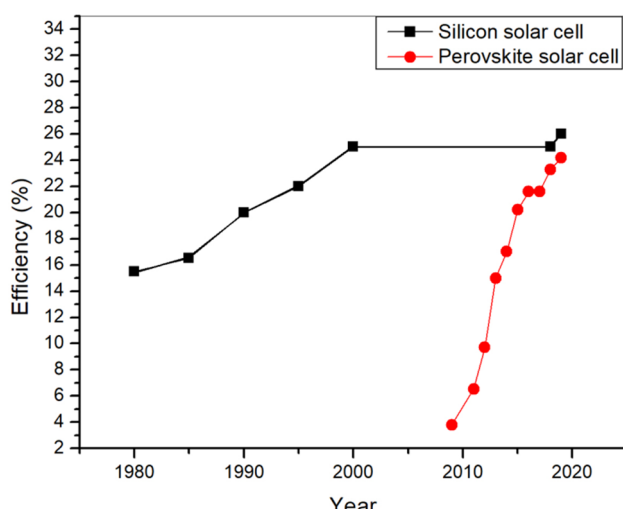


Fig. 2. Recorded Power Conversion Efficiency of the PSC in progressive years.

2017). Hwang et al. used a layer of Polytetrafluoroethylene, a hydrophobic polymer over the top of the PSC and noticed a minimal degradation for over 30-days in ambient air condition (Hwang et al., 2015). From all these works, it is concluded that it is one of the most rapidly growing PV cell with advancements taking place to date.

3. Structural properties of hybrid organic-inorganic perovskite materials

The Perovskite materials comprise the crystal structure similar to Calcium Titanate (CaTiO₃) and it follows the general formula of ABX₃ (where X is generally Oxygen, Nitrogen, Carbon or Halogen). Halide perovskites are of two types (i) Alkali halide based perovskite (ii) Organic-inorganic halide based perovskite. The Alkali halide based perovskite comprises of monovalent alkali cation (A) as Cs⁺, Rb⁺, k⁺, Na⁺ and Li⁺, divalent cation (B) as (Pb²⁺, Sn²⁺, Ge²⁺) and halogen anions (X) as Cl⁻, Br⁻, I⁻, F⁻. Organic-inorganic halide based perovskite has organic monovalent cation (A) as CH₃NH₃⁺, CH₃CH₂NH₃⁺, NH₂CHNH₂⁺ (Kim et al., 2014). Where 'A' ion having coordinate (0,0, 0,0, 0,0) in the crystal coordinate system and 'B' having coordinate (0.5, 0.5, 0.5) both represent cationic radii, with the size of A usually greater than B, and 'X' represents anionic site with coordinate (0.5, 0.5, 0) (Zhang et al., 2014). The cations 'A' and 'B' coordinates with 12 and 6 'X' anions creating cuboctahedral and octahedral geometries respectively. This halide based perovskite has attractive electrical, optical and magnetic properties that enable users to apply them in the field of solar cells (Sarukura et al., 2007). Ideal perovskite structure has the highest symmetry possessing cubic structure as shown in Fig. 3, the BX₆ octahedral network occupies the corner of the structure while A occupies the interstices. This BX₆ octahedral network plays a vital role in the determination of phase transition, bandgap and transport properties.

The perovskite formation tendency can be depicted by using Goldschmidt tolerance factor (t) which is given by -

$$t = \frac{R_A + R_X}{\sqrt{2(R_B + R_X)}} \quad (1)$$

$$\mu = \frac{R_B}{R_X} \quad (2)$$

where R_A, R_B, and R_X represent ionic radii of A, B cation and X anion respectively (Li et al., 2008). The value of the tolerance factor lies between 0.88 and 1.1 for a stable crystal structure of perovskite. It is usually expected that perovskite is stable if 't' lies within the specified range, but it is also seen that perovskite is not stable even if 't' is in the range of 0.8–0.9 (Li et al., 2004). An additional consideration for perovskite formation is taken into account, with the octahedral factor (μ), which is given by Eq. (2). It is used to determine the distortion and stability of the perovskite structure. The perovskite is stabilized for an octahedral factor ranging from 0.45 to 0.89 (Travis et al., 2016; Mitzi et al., 1999).

The most common absorber material used for PSC is methylammonium lead trihalide (MAPbI₃ where X is the halide which can be Cl, Br or I). The unit cell parameters increases from 5.68 to 5.92 to 6.27 Å as the size of the halide atom increase from Cl to Br to I. However, the aspherical shape and larger size of Methylammonium (MA) leads to the distortion in the network leading to phase transition with a decrease in the temperature, For T < 160 K, the orthorhombic structure, for 162.2 K < T < 327.4 K tetragonal structure, and for T > 327.4 K cubic structure is observed (Li et al., 2004). The bandgap of methylammonium lead halide usually lies within the range of 1.5–2.3 eV, where MAPbI₃ is a direct bandgap material with a bandgap of 1.55 eV approximately, whereas MAPbBr₃ has a comparatively wider bandgap of 2.3 eV for 800 nm absorption onset. FAPbI₃ (where FA is Formamidinium) shows comparatively narrower bandgap of 1.48 eV, signifying larger current extraction when employed as the absorber layer, but this material has shown lower stability. The structural

Table 3

Increment in efficiency in a progressive year.

PCE (%)	V _{oc} (v)	J _{sc} (mA/cm ²)	FF	Device Configuration	Year	Reference
3.8	0.61	11	0.57	Pt-FTO/Electrolyte solution/CH ₃ NH ₃ PbI ₃ /TiO ₂	2009	(Kojima et al., 2009)
6.54	0.706	15.82	0.586	Pt/Liquid Electrolyte/CH ₃ NH ₃ PbI ₃ (QD) / TiO ₂ /FTO	2011	(Hirayama et al., 1994)
9.7	0.888	17	0.62	Au/spiroOMeTAD/CH ₃ NH ₃ PbI ₃ /m-TiO ₂ /FTO	2012	(Minemoto and Murata, 2014)
15	0.993	20	0.73	Au/spiroOMeTAD/TiO ₂ /CH ₃ NH ₃ PbI ₃ /Glass	2013	(NREL PV Research Cell Record Efficiency Chart, 2019)
17.01	1.056	21.64	0.741	Au/spiro-MeOTAD/Cuboid MAPbI ₃ / MAPbI ₃ /m-TiO ₂ /c-TiO ₂ /FTO	2014	(Mitzl et al., 2010)
19.3	1.114	23	0.74	Au/Spiro-OMeTAD/Perovskite/m-Li _x TiO ₂ / Perovskite/ FTO	2014	(Ches et al., 2006)
20.2	1.06	24.7	0.775	Au/PTAA/Perovskite/(bl/m-TiO ₂)/FTO	2015	(Im et al., 2011)
20.5	1.1143	23.24	0.759	Au/Spiro-OMeTAD/Perovskite/m-TiO ₂ / bl-TiO ₂ / FTO	2016	(Kim et al., 2012)
21.6	1.14	23.7	0.78	Au/Spiro-OMeTAD/Perovskite/m-TiO ₂ / Perovskite/bl-TiO ₂ / FTO	2016	(Burschka et al., 2013)
22.1	1.11	25	0.817	FTO/TiO ₂ /m-TiO ₂ /perovskite composite layer/perovskite upper layer /PTAA/Au	2018	(Im et al., 2014)
22.7	1.14	24.92	0.792	FTO/d-TiO ₂ /mp-TiO ₂ /NBH/P3HT/Au	2019	(Jung et al., 2019)

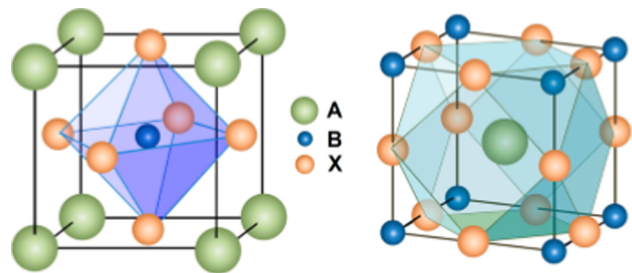


Fig. 3. ABX₃ perovskite structure showing (left) BX₆ octahedral and (right) AX₁₂ cuboctahedral geometry. Reprinted with permission from Ref (Kim et al., 2014). Copyright (2014) American Chemical Society.

properties of methylammonium lead halide also show variation depending upon the type of halogen atom used. On using smaller sized Br⁻ instead of I⁻ reduces the lattice constant thereby transiting into a more stable cubic phase. This fact is also evident by examining the crystal structure of MAPbI₃ and MAPbBr₃ which crystallize in the tetragonal form and cubic form respectively (Heo et al., 2013).

4. Progress in device architecture

Since the advent of the first PSC in dye-sensitized architecture, numerous works have been carried out in order to enhance the device stability and efficiency. The advancements in device architecture was one of the performance deciding factors in the evolution of the PSCs. In 2009, the perovskite was first used as a liquid electrolyte in dye-sensitized solar cell (DSSC) configuration; however, this configuration was not further used due to the low efficiency (3.8%) and unstable nature of the device due to the presence of the liquid electrolyte. Then this liquid electrolyte was replaced by Im et al. and the first solid-state PSC came into limelight, the implementation of the solid hole transport layer (Spiro-OMeTAD) was done, which not only improved the device efficiency (10%) but exhibited successful operation for 500 h also (Kim et al., 2012). The PSCs basically has five components: (i) a metal-based cathode, (ii) Hole transport layer (HTL) (iii) absorber layer (iv) Electron transport layer (ETL) (v) Transparent Conductive Oxide(TCO). The transport layer plays a vital role in deciding the performance of a PSC. The function of HTL is to collect holes from the absorber layer and transport it towards the cathode and block electrons. For any material to function as a hole transport material (HTM), it must have its highest occupied molecular orbital (HOMO) slightly higher than that of the perovskite absorber layer. Various HTMs used are: Spiro-OmeTAD, NiO, CuO, CuI, Cu₂O, PTAA, etc. The function of ETL is to collect electrons from the absorber layer and transport it towards anode and block holes. For a material to be used as an electron transport material (ETM), it must have its HOMO and LUMO (Lowest unoccupied molecular orbital) levels higher than that of the perovskite absorber layer. The ETMs must

possess high transmittance in UV–Vis region so that all the photons pass through it, and are maximum absorbed by the absorber layer. Various ETMs used are: TiO₂, SnO₂, SiO₂, ZnO, etc. Transport layers must exhibit the properties, such as good thermal stability, non-toxicity and must be resistive towards external degrading factors (Mahmood and Taqi, 2017; Jiang et al., 2019; Richardson et al., 2019). Currently, the efficiency of the PSC is raised up to 25.2% due to the enormous work carried to improve the device performance. This evolution in device performance. The various architectures like mesoporous, supermesoporous, regular and planar came into existence. A brief discussion on the evolution of device architecture along with its performance details is discussed in the following section.

4.1. Dye-sensitized structure

In 2009, the first PSC was fabricated by Kojima and coworkers. They used DSSC architecture. The perovskite sensitizer was used over TiO₂, which acted like a liquid electrolyte. They used fluorine-doped SnO₂ transparent conductive glass (FTO) as a substrate, transparent conductive oxide as a hole blocking layer, a counter electrode, a compact thin TiO₂ (c-TiO₂) and a microns thick mesoporous TiO₂ (m-TiO₂), which was sensitized over MAPbI₃ and MAPbBr₃ perovskite formed by spin coating the precursor solution created by using the equimolar concentration of methylammonium and lead halide. MAPbI₃ sensitized PSC exhibited the best performance in terms of efficiency, PCE = 3.81%, V_{oc} = 0.61 v, FF = 57%, J_{sc} = 11 mA/cm² and the solar cell using MAPbBr₃ sensitizer attained comparatively higher photovoltage with V_{oc} = 0.91 v, PCE = 3.13%, FF = 59%, J_{sc} = 5.57 mA/cm². Fig. 4(a) compares the spectra of IPCE PV cell of MAPbI₃/TiO₂ and MAPbBr₃/TiO₂ and (b) represents the I-V characteristic of MAPbI₃ and MAPbBr₃ PV cells under the exposure of 1.5AM irradiation. The current

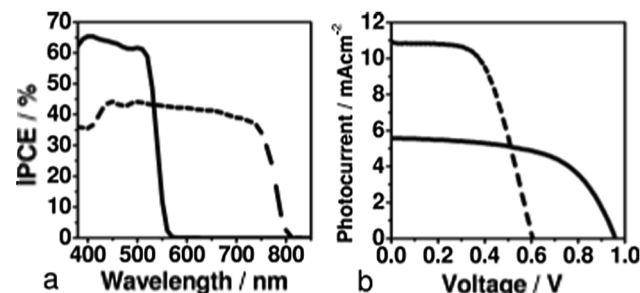


Fig. 4. (a) IPCE action spectra for photoelectrochemical cells using CH₃NH₃PbBr₃/TiO₂ (solid line) and CH₃NH₃PbI₃/TiO₂ (dashed line). (b) Photocurrent-voltage characteristics for cells using CH₃NH₃PbBr₃/TiO₂ (solid line) and CH₃NH₃PbI₃/TiO₂ (dashed line) under 100 mW cm⁻² AM 1.5 irradiation. Reprinted with permission from Ref. (Kojima et al., 2009). Copyright (2014) American Chemical Society.

density in MAPbI_3 is higher because it has a comparatively lower bandgap (1.5 eV) than MAPbBr_3 (2.3 eV). This work clearly indicated the potential of hybrid organic–inorganic perovskite materials (HIOPs) towards the PV application. However, this device was not further used because of poor device stability and low efficiency due to the presence of liquid electrolyte (Kojima et al., 2009).

In 2011, Im et al., used perovskite sensitized cell in DSSC configuration using 2–3 nm of MAPbI_3 quantum dots in order to coat the 3.6 μm thick m-TiO₂ layer. This device exhibited almost double the PCE obtained earlier with PCE = 6.54%, $V_{oc} = 0.706\text{V}$, FF = 58.6% and $J_{sc} = 15.82 \text{ mA/cm}^2$. This work indicated the high absorption coefficient of the perovskite (MAPbI_3) materials which is one of the most desirable features of materials to be used for PV application. However, the device performance was reduced by 80% as perovskite quantum dots dissolved in the liquid electrolyte after 10 min in continuous illumination.

4.2. Solid state mesoscopic structure

The instability raised due to the usage of liquid electrolyte was overcome by Hui-Seon Kim and co-workers in 2012. They reported the first solid-state mesoscopic structure heterojunction solar cell and attained a PCE of 9.7%. The view of the device cross-section is shown in Fig. 5.

This group used nanoparticles of MAPbI_3 as a light harvester, and deposited microns thick m-TiO₂ that filled the pores with the hole transport material, (spiro-MeOTAD). This created a direct contact between the hole transport layer and the sensitizer, whereas the rest of the HTL served as a capping layer over m-TiO₂, shown in Fig. 5(c). This capping layer further prevented shunting between ETMs and back contact. Under the illumination of AM-1.5, the device exhibited higher efficiency and better stability with PCE = 9.7%, $V_{oc} = 0.88\text{V}$, FF = 62%, $J_{sc} = 17 \text{ mA/cm}^2$. The usage of the solid-state hole conductor dramatically improved the efficiency and stability by operating successfully for 500 hr of continuous illumination (Kim et al., 2012). High-performance PSCs can be fabricated by reducing the thickness of the mesoporous layer which is beneficial for better pore filling (Wang et al., 2019). Mahmood et al. reported a PSC with a mesoporous ZnO film (440 nm thick). They adopted electrospraying process to fabricate and the device attained PCE = 10.8%, $V_{oc} = 1.01\text{V}$, FF = 67%, $J_{sc} = 16 \text{ mA/cm}^2$ (Mahmood et al., 2014).

4.3. Meso-superstructure structure

Based upon the previous work, Henry J. Snaith proposed a modified structure of the device where the m-TiO₂ was replaced by an insulating layer of m-Al₂O₃. They demonstrated that Al₂O₃ does not inject a

photoexcited electron but acts as a scaffold layer. The primary intention of this work was to study the behavior of electron transports through the perovskite layer and to examine the importance of m-TiO₂ in the functioning of PSC. The result came out to be surprising as not only the charge transport occurred at a faster rate but also the photocurrent was increased by the replacement. Their work revealed the fact that the phenomenon of charge collection was ten times faster with this modification. The open-circuit voltage arose from 200 to 300 mv, thereby increasing the PCE up to 10.9%, $V_{oc} = 0.98\text{V}$, FF = 63%, $J_{sc} = 17.8 \text{ mA/cm}^2$ (Tax et al., 2012). James M. Ball and co-workers in 2013, fabricated a PSC using mixed halide, $\text{MAPbI}_{3-x}\text{Cl}_x$ absorber and lowered the processing temperature from 500 to 150 °C for the first time and attained the PCE = 12.3%, $V_{oc} = 1.02\text{V}$, FF = 67%, $J_{sc} = 18 \text{ mA/cm}^2$. As earlier works suggested that the porous electron transport layer requires high-temperature sintering, so here researchers investigated its necessity by processing the absorber layer at a lower temperature. This led to the possibility of fabrication of PSCs upon a flexible substrate and multifunctional device architecture (Ball et al., 2013). It was seen that even processing at low temperature, all the primary functions of solar cells were fulfilled: absorption, carrier generation and collection along with minimum recombination loss. Therefore, this work suggested that the metal oxide scaffold which was fabricated over the perovskite layer could be processed in low temperature which further implied the compatibility of PSCs over a flexible substrate and also in multijunction architecture.

4.4. Regular structure

The favorable results obtained by mesosuperstructured configuration (MSSC) influenced the researchers to work more on this domain to acquire better results. After the properties like low trap density and longer diffusion lengths in HIOPs were revealed, it was indicated that thicker perovskite film could be used by replacing ETL in PSCs. Then the thickness of the absorption layer was increased expecting that it will improve the absorption at longer wavelength photon and will avoid the shunting of the electrodes also. Thus a device was created based upon the MSSC structure but it had a comparatively wider perovskite layer. This structure grabbed the attention of researchers across the world and was termed as a ‘Regular Structure’ because of the gained popularity. Heo et al. in 2013, proposed this configuration which had pillared perovskite structure, where the pores of the m-TiO₂ were completely filled with MAPbI_3 thereby, forming MAPbI_3 pillars. These pillars were further coated with thin polytriarylamine (PTAA) as a hole transport material (HTM) using Au as an electrode. The device achieved the PCE = 12% $V_{oc} = 0.997\text{V}$, FF = 72.7%, $J_{sc} = 16.5 \text{ mA/cm}^2$ (Heo et al., 2013). However, the device performance was limited due to the poor surface morphology. Then further modification was done in this

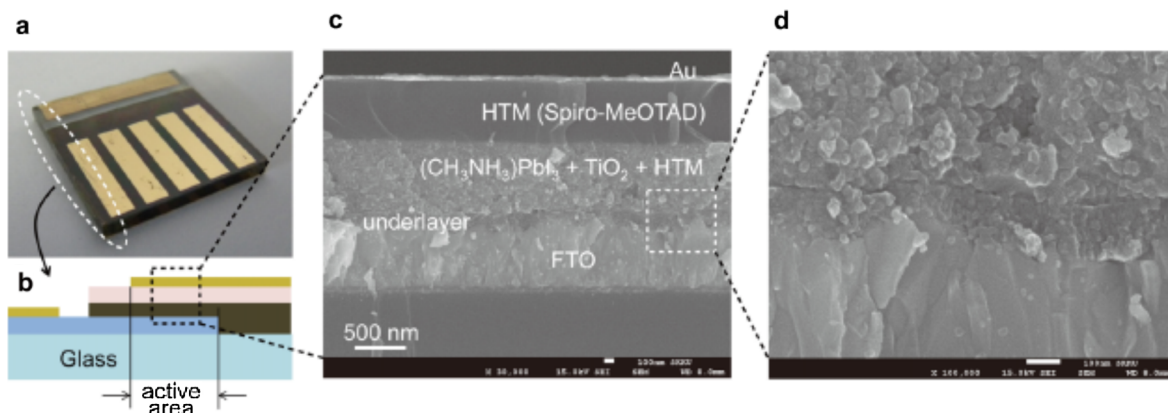


Fig. 5. (a) Real device picture (b) Cross-sectional view of the device (c) SEM image of the cross-section (d) Active layer-underlayer-FTO interfacial junction structure. Reprinted with permission from Ref. (Kim et al., 2012). Copyright (2012) Springer Nature.

structure by Burschka et al. by the implementing thicker perovskite film over thinner m-TiO₂ layer, a thin (50 nm) perovskite capping layer was also used over the top of m-TiO₂ (300 nm) layer using the two-step deposition method. They attained PCE = 15%, V_{oc} = 0.993v, FF =, J_{sc} = 20 mA/cm² (Minemoto and Murata, 2014). The same fabrication technique was later adopted by Im et al. who used 100 nm m-TiO₂ layer and raised the width of the capping layer to 150 nm and obtained comparatively better results with PCE = 17%, V_{oc} = 1.056v, FF = 74%, J_{sc} = 21.64 mA/cm² (NREL, 2019). A modification was further suggested by Giordano et al. when they doped the TiO₂ layer with Lithium and a thicker capping layer with thickness of 300 nm and attained PCE = 19.3%, V_{oc} = 1.114v, FF = 74%, J_{sc} = 23 mA/cm². Zhang et al. modified the film fabrication technique by using external-electric-field (EEF) supported the annealing process instead of using conventional annealing technique to enhance the performance of the PSC. Under the optimized condition, in electric field (E) of 2.5 v/μm, PCE of regular PSC improved from 16.77% to 19.18% and that of inverted PSC from 15.33% to 17.26%. This modification caused the better carrier extraction and superior film quality (Zhang et al., 2018).

4.5. Planar n-i-p heterojunction structure

This architecture was analogous to the thin film inorganic solar cells. The device structure had TCO cathode, an n-type ETL, intrinsic perovskite layer, p-type HTL, and a metal anode. This configuration eliminated the mesoporous layer from the regular structure. In 2012, Snaith et al. proposed the planar heterojunction PSC with mixed halide MAPbI_{3-x}Cl_x absorber layer, but unfortunately due to incomplete film coverage, shunting occurred and the device attained low PCE of 1.8%. Further to improve the film quality, Snaith et al. in 2013 came up with a dual-source co-evaporation of PbCl₂ and MAI and deposited the MAPbI_{3-x}Cl_x layer over c-TiO₂ layer and attained PCE = 15%, V_{oc} = 1.07v F = 67%, J_{sc} = 21.5 mA/cm² (Liu et al., 2013). The maximum efficiency in this architecture to date was given in 2018 by Dong Yang co-worker. They proposed a high efficiency planar n-i-p structure using EDTA complex tin oxide (SnO₂) as ETL, FAPbI₃ as the absorber layer with a slight amount of Cs doping for improvement of phase stability, Spiro-OMeTAD as hole transport layer (HTL) and attained PCE = 21.6%, V_{oc} = 1.11v, FF = 79.2%, J_{sc} = 24.55 mA/cm² (Yang et al., 2018). Mustafa Haider et al. in 2018 used a new HTL in this configuration whose schematic is shown in Fig. 6.

They used nickel phthalocyanine (NiPc) as a HTL and claimed it to be stable and cost-effective in comparison to spiro-OMeTAD. The device attained PCE = 12.1%, V_{oc} = 0.94v, FF = 73%, J_{sc} = 17.64 mA/cm². The device exhibited better stability by retaining 80% of the efficiency in the atmosphere upto 38 days. The comparison of the stability of the device with NiPc and Spiro-OMeTAD is shown in Fig. 7 (Haider et al., 2018). It is well reported that PSCs with organic HTMs although attain quite high initial PCE but undergoes rapid degradation. The PSCs with

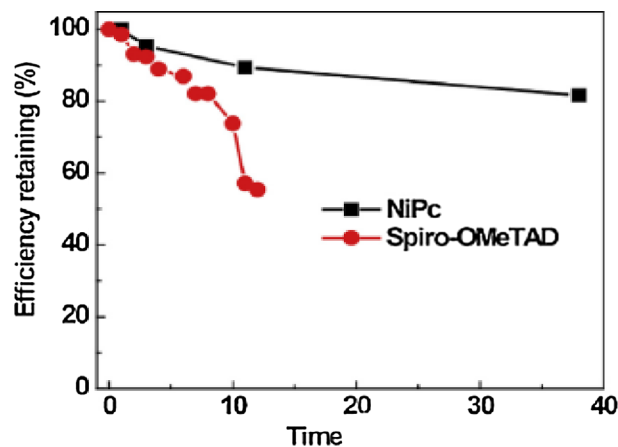


Fig. 7. Normalized efficiency decay curves of devices based on NiPc and commercial spiro-OMeTAD in air. Reprinted with permission from Ref. (Haider et al., 2018). Copyright (2018) Elsevier.

inorganic HTMs not only attain good PCE but also show comparatively better device stability. The most stable behaviour is exhibited by carbon based HTMs (Pitchaya and Natarajan, 2020).

Xingyue et al. demonstrated carbon-based planar n-i-p PSC with ETL as Ni-doped rutile TiO₂ and HTL as copper phthalocyanine (CuPc). They noticed that the Fermi level of ETL shifted upwards upon doping with Ni. It also increased the carrier mobility and conductivity with enhanced film morphology, thereby enhancing the charge transportation and extraction. This device displayed PCE of 17.46% which is claimed to exhibit the best performance among all the carbon-based PSCs, other parameters being J_{sc} = 22.41 mA/cm², FF = 0.726 and V_{oc} = 1.073v. The device retained its 97% of the initial efficiency for 1200 h (Liu et al., 2018).

4.6. Inverted planar structure

Along with the planar n-i-p structure and regular structure, the researchers from the PV community adopted a configuration from the field of organic solar cells, the planar p-i-n heterojunction structure. This configuration is usually termed as an inverted structure as it has a reverse sequence of ETLs and HTLs from the regular structure. This structure has an anode (TCO), a p-type HTL, perovskite intrinsic layer, an n-type ETL and a metal cathode. In 2013, Jeng et al. fabricated planar p-i-n PSC by using MAPbI₃ as an active layer, BCP and Polypolystyrene sulfonate (PEDOT:PSS) as electron transport and hole transport material, respectively with the device structure ITO/PEDOT:PSS/MAPbI₃/C₆₀/bathocuproine (BCP)/Al. The device exhibited PCE of 1.6% which was further raised to 3.9% upon the replacement of C₆₀ with phenyl-C₆₁-butyric acid. Later Snaith et al.

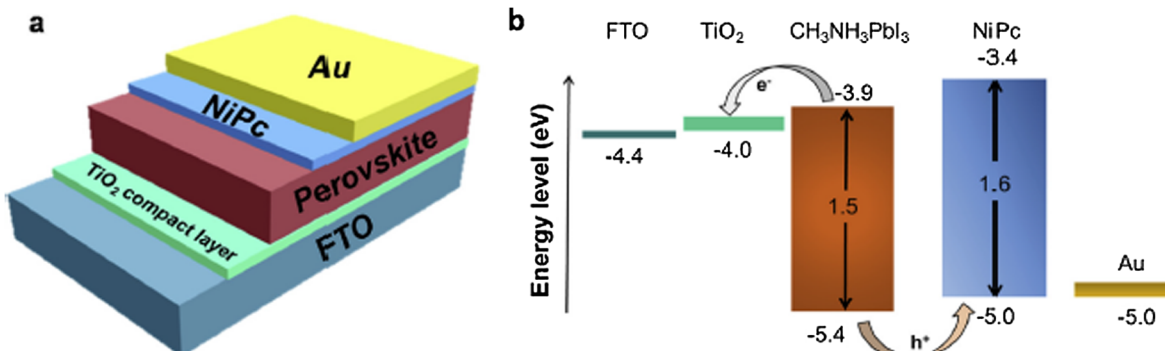


Fig. 6. (a) Schematic of n-i-p planar structure using NiPc as HTL (b) Normalized efficiency decay curves of devices based on NiPc and commercial Spiro-OMeTAD in air. Reprinted with permission from Ref. (Haider et al., 2018). Copyright (2018) Elsevier.

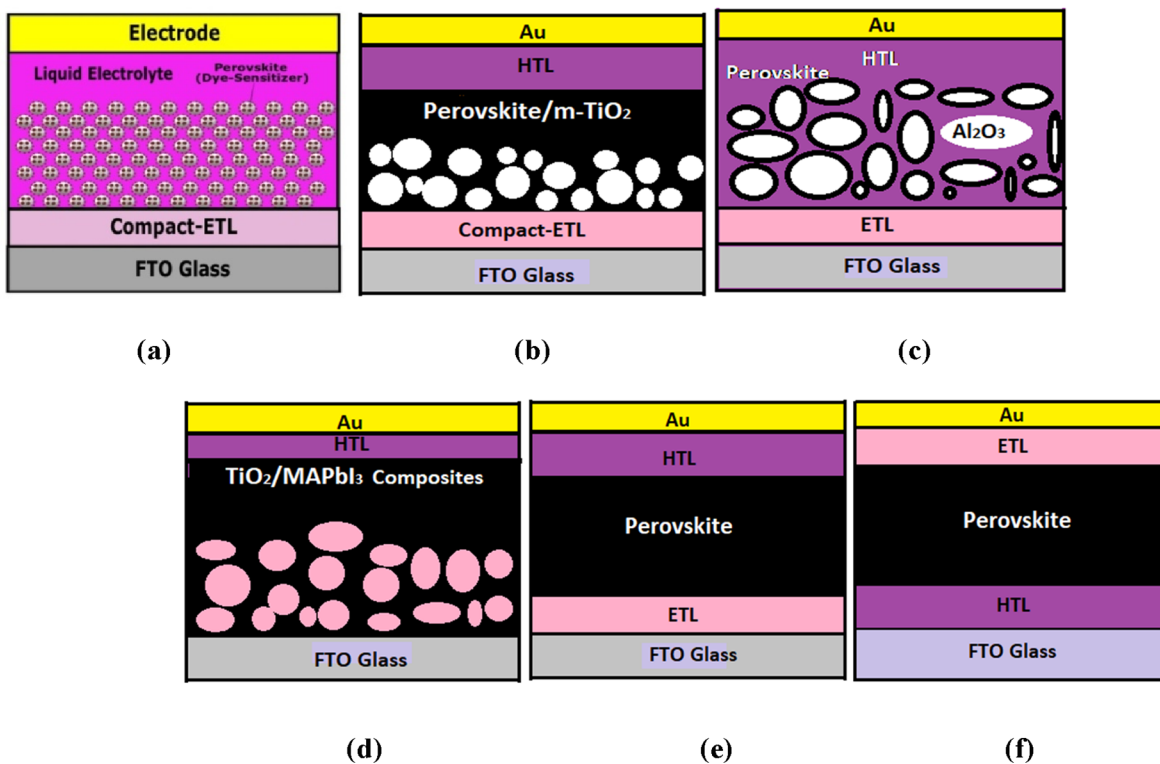


Fig. 8. Device architecture cross section: (a) DSSC (b) Mesoporous (c) Supermesostructure (d) Planar nip (e) Planar pin (inverted planar) structure.

acquired PCE of 9.8% with the incorporation of mixed halide and replacing the HTL by PC₆₁BM with the structure of FTO/PEDOT:PSS/MAPb I_{3-x}Cl_x/PC₆₁BM/TiO₂/Al (Docampo et al., 2013).

In 2018, Jie Tang et al. formed a high performance inverted planar structure using a new HTL and obtained better results by achieving better transparency and low loss of photon flux. They used NiO nanocrystals prepared by the solvothermal method as HTL, PCBM/BCP as ETL, MAPbI₃ as an absorber layer and Au as an anode. They varied the thickness of the NiO HTLs to 30 nm, 55 nm, 70 nm, 100 nm, and 170 nm and obtained the best performance in the structure with NiO layer thickness of 55 nm. The device attained PCE = 15.47%, V_{oc} = 1.06V, FF = 75.02% and J_{sc} = 19.41 mA/cm². They also compared two HTLs PEDOT: PSS and NiO nanocrystal and claimed NiO nanocrystal to exhibit superior performance (Tang et al., 2018). Schematic illustration of the above-mentioned architectures is shown in Fig. 8.

5. Fabrication techniques in PSCs

The potential of the PSCs is evident from their rapid increment in PCE from 3.8% to 25.2% within a decade. The path of efficiency enhancement went through the modification in device architecture, incorporation of new carrier transport materials (ETLs and HTLs) and improvement in the absorber layer and more. The improvement in the absorber layer is done by the modification in the anionic and cationic components, (like using FA along with MA and using mixed halides (Eperon et al., 2014; Bi et al., 2017; Aharon et al., 2015), addition of the performance booster additives (like Cs and Rb) (Park et al., 2015) and improvement in the perovskite film fabrication technique. Apart from the organic and inorganic component in the perovskite layer, the structural and optoelectronic properties of the film also depend upon the added solvent, film fabrication technique, annealing temperature and atmospheric conditions such as temperature, moisture, oxygen, etc. Usually a fine control over the stoichiometry, grain structure and crystallographic phase of the perovskite layer is required to fabricate an efficient PSC (Jeon et al., 2015; Sun et al., 2016; Jeon et al., 2014). As these parameters depend upon film deposition technique to a great

extent, wide research has been carried out by the researchers to develop the various fabrication techniques (Chiang et al., 2016; Yang et al., 2017; Cherrette et al., 2017; Deng et al., 2015; Wang et al., 2019; Schultes et al., 2019; Saliba et al., 2018). In the following sections, we discuss the various film fabrication and PSC manufacturing techniques used for large scale production.

5.1. Perovskite film fabrication techniques

The most decisive factor in determining the performance of the PSCs is the quality of perovskite film. To date, various methods have been established to fabricate an improved quality of perovskite film. The properties of the film like morphology, uniformity, crystallinity and phase purity depend upon the processing techniques which have a direct impact on the performance of PSC. The X-ray diffraction studies reveal that the activation energy of perovskites (56.6–97.3 kJ mol⁻¹) is much lesser than that of silicon (280–470 kJ mol⁻¹) (Moore et al., 2015; Köster, 1978). Low activation energy suggests that the perovskites can be synthesized using a variety of low-temperature processes, which are discussed in this section. The fabrication technique must give complete film coverage over the substrate as incomplete film coverage might lead to the formation of shunt paths by creating direct contact between ETLs and HTLs. Secondly, if the active layer does not have full coverage then the incident light may pass through directly without any absorption. The various perovskite film deposition techniques are discussed in this section.

5.1.1. Single-step deposition

This is the most widely used technique because of the simplicity and low-cost requirement. In this technique, the precursor solution is generally spin-coated over the TiO₂ scaffold. Here, the organic and inorganic solutes together are mixed in an aprotic polar solvent like DMF, DMSO, GBL, DMAc, and NMP (Jeon et al., 2014; Gardner et al., 2016; Noel et al., 2017; Hendriks et al., 2017; Yang et al., 2019) resulting in a precursor solution. All the solvents here have a high boiling point and low vapor pressure at room temperature. Due to strong ionic interaction

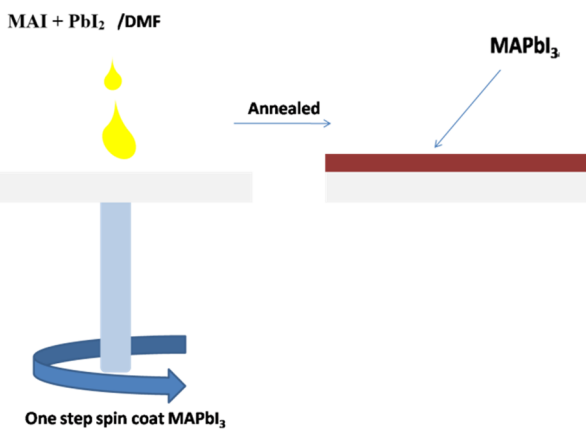


Fig. 9. The schematic representation of the One-Step deposition technique.

among halogen anions and metal cations, a uniform and a crystallized layer of perovskite is formed. The formation of a uniform layer is due to the convective self-assembly and the evaporation of solvent occurred during the spinning. After the precursor solution is spin-coated over the substrate, annealing is done at a temperature of 80 °C to 150 °C (Jeon et al., 2015; Sun et al., 2016; Jeon et al., 2014). However, simply spin coating never yields uniform and homogeneous layer over a large area. A study revealed that uniformity of the perovskite layer is dependent upon the thickness of the TiO₂ layer (Eperon et al., 2013). This deposition method requires a lesser number of processing steps, making the procedure easy to execute, however it forms a non-uniform layer with pinholes due to slow crystallization. The uncontrollable growth of film along with the variable morphology for grown crystals was later overcome by a 2-step sequential deposition technique (Zheng et al., 2015). The schematic representation of the One-Step deposition technique is represented in Fig. 9.

5.1.2. Two-step sequential deposition

One-step deposition method produced the perovskite film with poor surface coverage showing unavoidable non-uniformity. To avoid this Mitzi et al. proposed a two-step solution deposition method (Liang et al., 2013). They firstly deposited film over nanoporous TiO₂ layer by spin coating the solution of DMF at 70 °C. Secondly, the layer was converted to a perovskite layer upon reaction with MAI solution. In this method, the layer of MAI is added by (i) spin coating the solution of MAI over PbI₂ layer (ii) dip coating the PbI₂ film over MAI solution. When MAI solution is spin-coated over the PbI₂ film the spinning speed and spinning time play an impactful role in determining the quality of the perovskite layer formed (Huang et al., 2018). Whereas in the case of dip coating of the MAI layer, the dipping time and dipping concentration play a major role. Im et al. studied the impact of concentration of MAI over surface morphology and obtained the relation that the grain size reduces with an increase in the MAI concentration (Im et al., 2014). Although this method produces better film as compared to the one-step deposition method, it does have some shortcomings. The main drawback arises from the interrelation between surface roughness and grain size. As the grain size increases, the surface roughness also increases. A rough perovskite film with larger grain size leads to high leakage current and high surface recombination loss, whereas a smooth film with small grain suffers small carrier lifetime and short diffusion length. Therefore, an appropriate composition has to be fixed. Secondly in the case of partial conversion of PbI₂, specifically in planar structure, the residual PbI₂ reduces the light absorption and also hinders carrier transport which further degrades the performance of the PSCs (Wu et al., 2014; Zhou et al., 2015). In order to tackle such issues, the solvent engineering technique was applied. The schematic representation of the Two-step deposition technique is represented in Fig. 10.

5.1.3. Rapid deposition crystallization

In this technique, an antisolvent is dripped within a short time delay after the perovskite layer is deposited over the substrate. Then, by the addition of antisolvent in the perovskite layer, the growth rate and nucleation of the film are increased. This creates a uniform film with larger grain crystals (Mei et al., 2014). Various antisolvents generally used are chlorobenzene, benzonitrile, ethanol, benzene, xylene, methanol, ethylene glycol, toluene, and acetonitrile.

5.1.4. Lewis base adduct method of lead (II) iodide

Ahn et al. in 2015 proposed the fabrication of MAPbI₃ film by lewis base adduct method of lead (II) iodide. They dissolved PbI₂ in N,N-dimethylformamide (DMF) by preparing the equimolar solution of MAI in N,N-dimethyl sulfoxide (DMSO). The adduct of MAI·PbI₂·DMSO and PbI₂·DMSO is formed due to the reaction between Lewis acid PbI₂ and Lewis base DMSO and/or iodide (I⁻). Spin coating of DMF solution comprising PbI₂, DMSO and MAI in equimolar concentration forms transparent adduct film. During the spinning, Diethyl ether is added so that DMF gets completely removed and the formation of 1:1:1 adduct film takes place. Further, the film gets converted into dark brown upon heating at 65 °C for 1 min because of the elimination of volatile DMSO from adduct Fig. 11.

This adduct-method gave MAPbI₃ film with high charge carrier extraction, slow recombination rate and carrier mobility of 3.9×10^{-3} cm²/(Vs). The carrier mobility obtained by this method is larger than that of obtained by solution processing technique (3.2×10^{-2} cm²/(Vs)). The PSC fabricated by this method gave PCE of 19.7% (Park, 2015).

5.1.5. Vapour assisted solution processing

Qi Chen et al. in 2014 demonstrated a novel low-temperature vapor assisted process to deposit perovskite film. This method was basically the modified version of the two-step sequential deposition technique. The incorporation of MAI was done via vapor deposition technique over the PbI₂ seed layer which is deposited by spin coating, where the MAI vapor was formed at 150 °C in an inert environment. The fabricated film was uniform, had full coverage and grain size up to microns. The film exhibited minimal roughness with 100% precursor transformation. This technique avoided the delamination issue arising in two-step methods while removing from MAI solution or washed for while removing from MAI solution or washed from IPA solution (Chen et al., 2014).

5.1.6. Thermal evaporation

Snaith et al. fabricated the first vacuum-deposited film where he co-evaporated the organic and inorganic species (Liu et al., 2013). They prepared CH₃NH₃PbI_{3-x}Cl_x by evaporating, MAI and PbI₂ precursor salts evaporated simultaneously from different sources at 10⁻⁵ bar deposited at the ratio of 4:1. They placed sensors above the ceramic crucible, and fabricated the film in the nitrogenous environment in glove box. Vapor deposited film came out to be exceptionally uniform with crystalline features over the length scale of 100's of nanometers, whereas spin coating film rendered incomplete film coverage with crystalline 'plalets' of micron range. In this method, the deposition rate of MAI was hard to control. However, this could be overcome by adopting the sequential deposition method where PbI₂ was firstly coated followed by deposition of MAI vapor. Snaith further fabricated two cells using both methods, i.e. vapor evaporation and solution-processed, and observed the PSC prepared from vapor evaporation to exhibit superior performance.

5.1.7. Pulse laser deposition (PLD)

Liang et al. in 2015 fabricated inverted PSC using a pulsed laser deposition technique. They deposited the PbI₂ layer using PLD and MAI was deposited using a simple spin coating method. The technique is easy and precise, had operational simplicity, and gave a specific control over the thickness of the layer deposited. The asymmetric nature

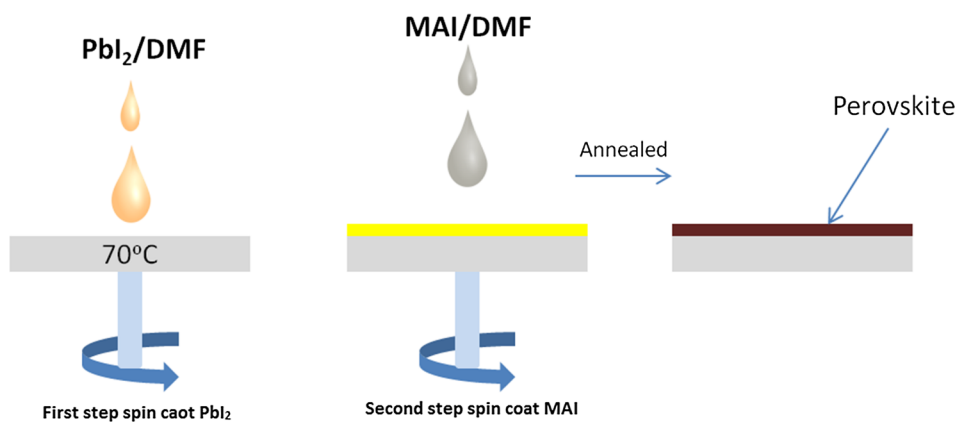


Fig. 10. Schematic representation of Two-Step deposition technique.

permits the stoichiometric mass transfer of material from target to substrate. The parameters that have to be controlled in PLD is pulse repetition rate, substrate temperature, beam energy density, and pressure. During the deposition, was powdered in isopropanol baked at 100 °C pressed at the pallet, followed by sintering at 120 °C under a nitrogenous environment for 8 hr. The deposition of MAI layer was done by the spin-coating technique. The fabricated film was compact, crystalline, uniform and continuous with larger grain size (Liang et al., 2016).

5.1.8. Electrospray-assisted deposition

This technique enables us to fabricate a stable and moisture resistant PSC at the ambient humid condition. In this technique, the PbI_2 layer is deposited on TiO_2 coated FTO glass substrate by simple spin coating. Further, the MAI is electrospray by pumping via capillary needle at higher voltage while generating a monodispersed charge droplet in Taylor cone-jet mode. This electrospraying deposition technique enables to control the film formation reaction rendering a uniform, smooth surface morphology, the stable film with moisture-

resistant nature at ambient condition. It is a scalable technique, which offers accurate control over the quantity of material necessary for the deposition. Moreover, this technique avoids the loss of material that occurs during solution-processed technique. The surface of the film fabricated by the solution-processed method is hydrophilic in nature, which gives the low contact angle with the water droplet whereas the film fabricated by this technique has an extremely smooth surface which is hydrophobic in nature. In order to test the stability of the electrosprayed film, the water droplet was sprayed over it followed by its heating at 100 °C. This leads to the degradation of PbI_2 , but later regained the crystalline feature by the transformation in color from yellow, black to dark brown. The result of XRD in the films before and after water spraying was almost identical which indicated the occurrence of self-healing mechanism (Kavadiya et al., 2017).

5.2. Large scale manufacturing techniques

The easy manufacturing and outstanding electronic properties of the hybrid organic-inorganic perovskite materials with great device

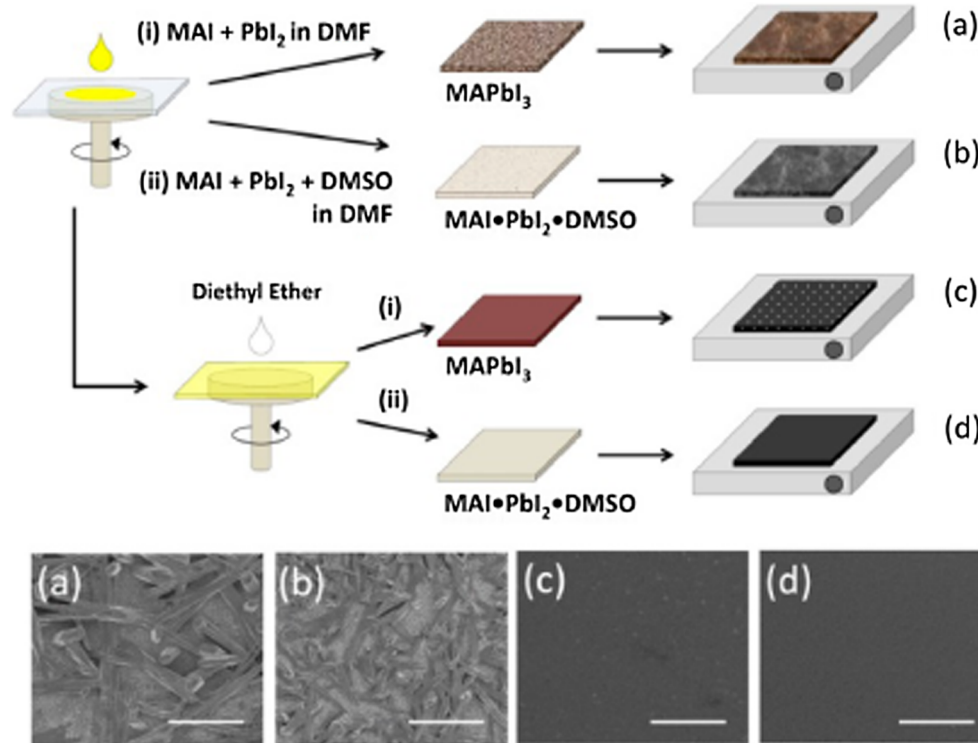


Fig. 11. Schematic representation of fabrication procedure and plane view scanning electron microscopy (SEM) image for the MAPbI₃ perovskite layers obtained by direct one-step spin-coating of the DMF solution containing (a) MAI and PbI_2 or (b) MAI, PbI_2 , and DMSO. Panels (c) and (d) were prepared by same solution as that in panels (a) and (b), but diethyl ether was dripped during the film spinning. Reprinted with permission from Ref. (Park, 2015). Copyright (2015) American Chemical Society.

performance initiated the idea of successful commercialization of the PSCs. Till now for research purposes in laboratories spin coating is being widely used. However, to fabricate large-area PSC the spin coating technique cannot be adopted. Therefore several methods are being looked up for large scale production of PSCs some of them are discussed below.

5.2.1. Inkjet printing

Inkjet printing technology is taken from newspaper printing and graphics technology. This is the digitalized form of the conventional printing process where desired patterns to be printed are controlled by computers. This being a non-contact process eliminates the requirement of a particular material or shape of the substrate (Huang et al., 2018). The advantage of this technique over other deposition techniques is that it offers mask-less on-demand patterning, low cost, efficient use of material, scalable, provides high-resolution printing and has freedom of design (Peng et al., 2017). This method was first used by Wei et al. in 2014, where they fabricated the first planar PSC with inkjet printing technique with nanocarbon HTL and had precise control over interface and patterns. They compared two ways to fabricate MAPbI_3 layer using this technique, among which the method where they prepared mixed ink using MAI and carbon that was printed over the PbI_2 , after heating for one hour the PbI_2 layer was transformed into MAPbI_3 layer showed better results (Wei et al., 2014). S.G. Hashmi et al. examined the stability of inkjet-printed PSC fabricated in the open air with intense UV exposure. They obtained impressively good stability under 1.5 Sun UV illumination for 1002 h in air by application of simple epoxy glue sealing of the PSCs (Yang et al., 2017). Mathies et al. fabricated a triple cation based PSC using this method and successfully attained a stable performance shown in Fig. 12.

They used 10% Cesium in FA and MA with $\text{Pb}(\text{I}/\text{Br})_2$ to deposit the

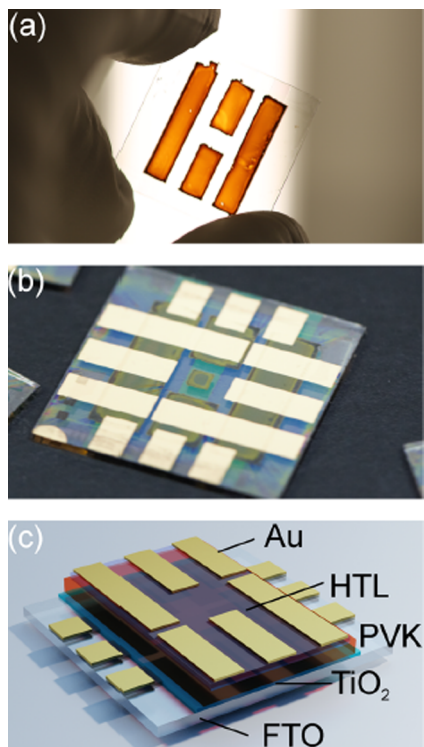


Fig. 12. (a) 520 nm thick inkjet-printed perovskite layer on FTO/TiO₂-coated glass substrate (b) Photograph of inkjet-printed perovskite solar cells. The substrate contains eight cells with each $3 \times 3 \text{ mm}^2$ active area. (c) Schematic diagram of the solar cell stack, denoting the different layers: glass/FTO/TiO₂/triple cation perovskite (PVK)/spiro-MeOTAD (HTL)/Au. Reprinted with permission from Ref. (Mathies et al., 2018). Copyright (2015) American Chemical Society.

active layer using inkjet printing technology, the PSC exhibited stability towards moisture and heat (Mathies et al., 2018). Therefore it can be said that this technology is capable of producing stable and durable PSCs with good production scalability.

5.2.2. Drop casting

Drop casting of the perovskite precursor solution over the screen-printed scaffolds is a productive method for the fabrication of PSC modules. The procedure is a low cost, easy, and poses a high production rate enabling large scale production (Mei et al., 2014). This method is executed by simply transferring the perovskite precursor solution over the substrate followed by heating in order to remove excess solvent. No other special equipment is required in this method. Fabrication of PSC using drop casting was first used by Han et al. in 2014, where the perovskite layer was directly deposited over m-ZrO₂ and m-TiO₂ double scaffold layer, thereby eliminating the requirement of HTL. They added an additive in the precursor solution, namely 5-aminovaleric acid, resulting ((5-AVA)_x(MA)_{1-x}PbI₃) perovskite film which had enhanced pore filling and low defect concentration. Later Niu et al. (Niu et al., 2015) used a solution-based hot casting method to fabricate the perovskite layer. They obtained a pinhole-free uniform layer with a device efficiency of 18% in planar architecture.

Anye Mei et al. used this technique to fabricate a $10 \times 10 \text{ cm}^2$ Perovskite the panel, in which 10 cells were serially connected with a total area of 49 cm^2 . The screen-printed TiO₂/ZrO₂/carbon triple-layer over the scaffold then drop cast ((5-AVA)_x(MA)_{1-x}PbI₃) at the carbon side. The panel exhibited stable performance for over 1000 h with PCE of 10.4%. However, the PCE attained by this method is still much lower than that attained by the conventional spin coating technique. In order to get a controlled production rate it is advisable to construct an auto production line (Mei et al., 2014).

5.2.3. Doctor blade coating

This technique is a low cost, simple to execute, has high productivity and is compatible with roll-to-roll fabrication which makes it appropriate for large scale production of PSCs. The doctor blade technique is performed by simply pouring a fixed amount of perovskite precursor solution over the substrate, followed by swiping the glass blade linearly with a high speed, without the requirement of any specific instrument. During the doctor blade deposition, it is advisable to hold the substrate at elevated temperature for obtaining pinhole-free, uniform, and smooth film. The heated substrate enhances the solvent evaporation rate, promotes nucleation and crystal growth. The application of the airflow over the substrate also helps the solvent to evaporate rapidly (Wang et al., 2019). The crystallization and the thickness of the film can be controlled in this method by regulating the gap between blade and substrate, the concentration of precursor solution, speed of movement of blade (Zhang et al., 2018). Yehao Deng et al. firstly used this technique to fabricate PSC which had device architecture of ITO/HTL/MAPbI₃/[6,6]-phenyl-C61-butyric acid methyl ester (PC60BM)/C₆₀/2,9-dimethyl-4,7-diphenyl-1,10-phenanthroline (BCP)/Al. This group attained PCE of 15.1% and reported the film to have large and continuous grain-sized. The remarkable point about this technique is that it requires a comparatively lesser amount of precursor solution as compared to conventional spin coating techniques (Deng et al., 2015). Later Yehao Deng et al. again used the Doctor blade technique to fabricate colourful PSC using perovskite photonics nanostructure and attained efficiency close to the optimized PSC (Wang et al., 2019). Shirazi et al. employed this technique to fabricate a HTL free PSC with Al-doped ZnO nanostructures as ETL and carbon paste as an electrode. In this case, the carbon electrode was doctor bladed followed by annealing at 100 °C (Shirazi et al., 2018). Many works have been carried out using this technique to fabricate PSCs with large areas with optimized PCE (Back et al., 2016; Razza et al., 2015). The schematic of this technique is represented in Fig. 13 (Wang et al., 2019).

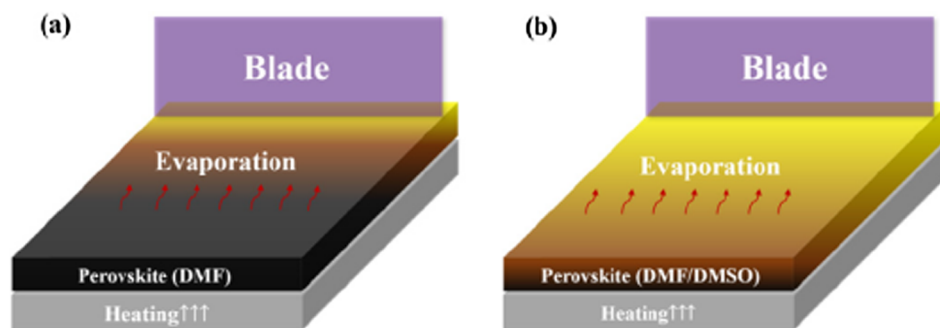


Fig. 13. Schematic diagrams of perovskite films formed by doctor blade coating with (a) DMF-based and (b) DMF/DMSO-based precursor solutions. Reprinted with permission from Ref. (Wang et al., 2019). Copyright (2019) Elsevier.

5.2.4. Slot die coating

This technique is analogous to the previously stated doctor blade coating technique; the only change is that the blade is supplied with an ink reservoir which spreads the precursor solution over the substrate. The film quality attained is better in this technique as compared to the doctor blade technique, however, the amount of precursor solution required in slot die coating is much larger. Vak et al. (2015) used 3D-printer connected with a slot-die coater, this enables precise control over the position of the coating tip. They fabricated the PbI_2 layer using the Slot die coating technique in the two-step sequential deposition of perovskite film and used the gas-quenching process to attain a pin-hole free and uniform layer. The second step of perovskite layer fabrication i.e., deposition of the MAI layer is generally done either by dip coating or by spin coating, however, slot dies coating can also be employed successfully for this purpose. Burkitt et al. (Daniel et al., 2019) fabricated all four-layer using this technique including HTL, ETL, perovskite and mesoporous layer in a simplified way. Verhees et al. used this technique along with laser patterning to fabricate a large area panel of dimensions $12.5 \times 13.5 \text{ cm}^2$ and attained PCE of 10% (Di Giacomo et al., 2018).

5.2.5. Spray coating

This technique is widely used in the fabrication of oxide thin films and organic photovoltaic cells. The technique of spray coating can also be used in the fabrication of perovskite thin films (Barrows et al., 2014; Yeo et al., 2019; Bishop et al., 2018). The experimental setup required for this technique is the same as inkjet printing. It has two systems, atomizing and deposition system which is both connected by quartz nozzle through which we can add perovskite precursor solution. The atomizer converts perovskite solution into tiny droplets, then a gas stream of low pressure guides the droplets into the substrate, as the solvent gets evaporated the deposition of perovskite film over the substrate is accomplished. Depending upon the way of dispersion of droplet over substrate this method is classified as follows: (i) Ultrasonic spraying (by ultrasonic vibration) (ii) Pneumatic spraying (by Fast gas flow) (iii) Electrospraying (by electrostatic repulsive force) (Zhang et al., 2018). In the fabrication of perovskite and ETL layers ultrasonic spraying has been adopted (Hsieh et al., 2018; Bai et al., 2016; Habibi et al., 2017). Barrow et al. used this method in 2014 for the first time for fabrication of a planar perovskite solar cell with mixed halide perovskite absorber layer ($\text{CH}_3\text{NH}_3\text{PbI}_{3-x}\text{Cl}_x$) and attained PCE of 11% in single-step deposition (Barrows et al., 2014). The quality of the perovskite layer being deposited can be controlled by checking the characteristic of precursor liquid droplets during spray coating. Surface tension is one of the deciding factors for the film quality deposited by this technique. The large surface tension will lead the accumulation of perovskite precursor solution in the form of the spherical cap over the substrate leading to poor wettability. It is advisable to keep the substrate at a high temperature in order to raise the evaporation rate of the solvent while deposition (Huang et al., 2018) schematic shown in Fig. 14.

6. Degradation in PSCs: Stability issue

The PSCs are said to be the future generation of the solar cell because of its rapid advancement in the performance in such a shorter span of time. Till now efficiency comparable to Silicon solar cell has been successfully attained, but the improvement in the device stability are still to be ensured. Even though comparable efficiency has been attained, but full replacement of the Silicon PV cells from the market cannot be done as the lifetime of Silicon cells are as high as 25 years, whereas the PSCs have shorter life span ranging from few days to months and maximum up to a year (Wang et al., 2019). The component of PSCs seems to degrade very quickly which ultimately leads the device to collapse. The factors affecting the stability of PSCs are oxygen, moisture, temperature, illumination, biasing and UV and more summarized in Fig. 15 (Niu et al., 2015). However, the moisture and oxygen contact into PSCs can be avoided by simply using encapsulation in PSCs (Hwang et al., 2015; Kosasih and Ducati, 2018; Matteocci et al., 2014). The encapsulation raises the overall cost of the device and is incapable to protect the device from harmful effects imposed by other factors like illumination, biasing, light and heat (Asghar et al., 2017). In the following sections, the impact of the above-mentioned factors is discussed briefly.

6.1. Moisture and oxygen effect

The first issue, which arises in PSCs is the interaction of the perovskite layer with water molecules and oxygen. This is an unavoidable phenomenon that occurs even during the procedure of cell testing and assembling. The MAPbX_3 layer breaks down into the constituent components upon reacting with water molecules. The illustration of the breakdown pathway is discussed taking $\text{CH}_3\text{NH}_3\text{PbI}_3$ layer. It degrades initially into original $\text{CH}_3\text{NH}_3\text{I}$ and PbI_2 which ultimately produces aqueous HI , solid PbI_2 and volatile CH_3NH_2 (Shaikh et al., 2017; Mehmood et al., 2017). The instability due to moisture generally arises due to the hygroscopic nature of the amine salts. $\text{MAPbI}_{3-x}\text{Cl}_x$ and MAPbI_3 both exhibit similar behavior in the presence of moisture, where MA sublimates leaving only PbI_2 behind (Philippe et al., 2015; Kwon et al., 2014). The material has hydrophilic nature due to which it readily absorbs water from surrounding which further leads to the formation of products similar to hydrates $(\text{CH}_3\text{NH}_3)_4\text{PbI}_6 \cdot 2\text{H}_2\text{O}$ (Christians et al., 2015). The degradation pathway is exhibited in the following equations (Zhang et al., 2018). It is stated that water molecules behave as a catalyst for the degradation to take place. The perovskite film generally transforms from dark brown color to light yellow color on its exposure to ambient conditions.

The optoelectronic properties of the perovskite film depend upon the crystal structure. The occurrence of phase transformation in perovskite distorts the crystal structure which degrades the cell performance. This fact was further verified when Jeffrey A Christians et al. reported the change in the crystal structure, causing a change in the

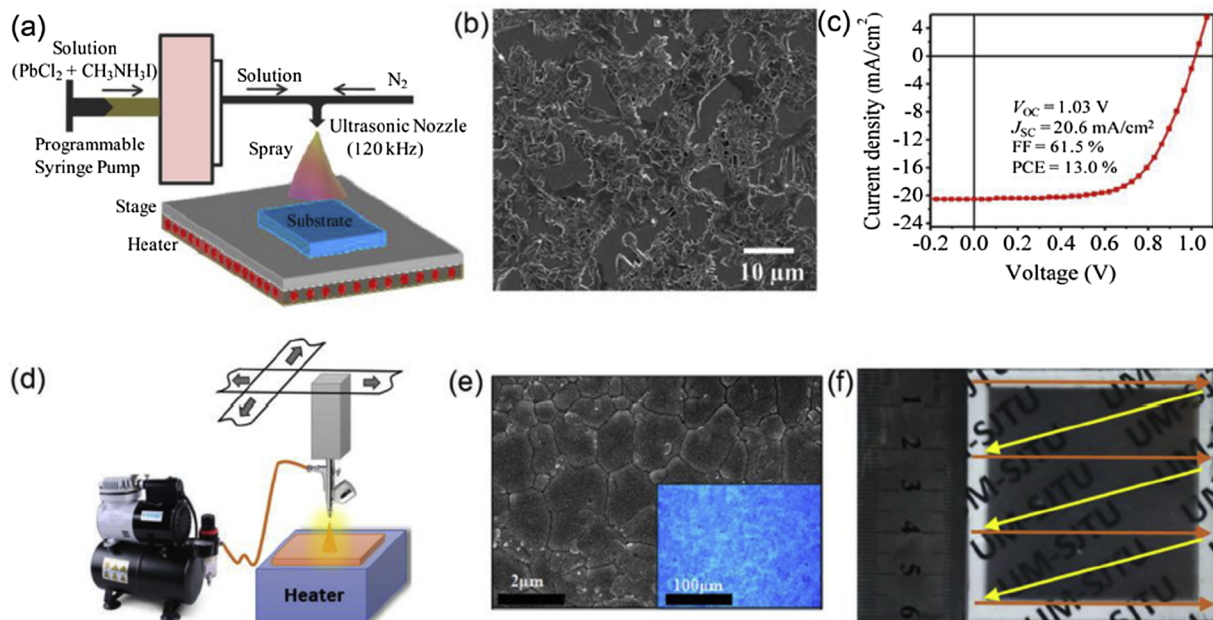


Fig. 14. (a) Schematic illustration of ultrasonic spray-coating process, (b) SEM image of spray-coated perovskite film at 90 °C and (c) J-V curves of the champion device under dark and standard illumination conditions. (d) Illustration of improved spray coating system, (e) SEM and optical image (inset) of perovskite film prepared with the method of spray coating at a substrate temperature of 25 °C and (f) the deposition pattern based on a zigzag movement of the spray nozzle over the substrate. Reprinted with permission from Ref. (Yang et al., 2017). Copyright (2015) Elsevier.

absorption spectrum of the perovskite film (Christians et al., 2015). The presence of the constituent layers around the perovskite layer also has a considerable impact on the stability of the cell. Like using material as HTL with hydrophobic properties will enhance the stability as compared to Spiro MeoTAD and PTAA. Alternatively, stability can be improved by using a coating of a hydrophobic layer above the cell. Hwang et al. obtained enhanced stability using facile hydrophobic passivation technique, here they used Polytetrafluoroethylene coating and reported negligible degradation for up to 30 days in an ambient atmosphere (Hwang et al., 2015). Naghadeh et al. showed exposure of perovskite

film to heat and moisture leads to rapid degradation by loss of the organic component (e.g. MA) thereby leaving only the traces of PbI_2 behind from the crystal structure (Bonabi Naghadeh et al., 2018). The degradation due to moisture was overcome by the addition of a thin blocking layer of Al_2O_3 between the HTL and perovskite layer (Mei et al., 2014). Karunadasa et al. used 2D hybrid perovskite $[(\text{PEA})_2(\text{MA})_2(\text{Pb}_3\text{I}_{10})]$ where PEA is $\text{C}_6\text{H}_5(\text{CH}_2)_2\text{NH}_3$. They spin-coated the film in ambient air and obtained better stability as compared to MAPbI_3 . The master film retained the crystal structure even after 46 days whereas MAPbI_3 degraded completely (Smith et al., 2014).

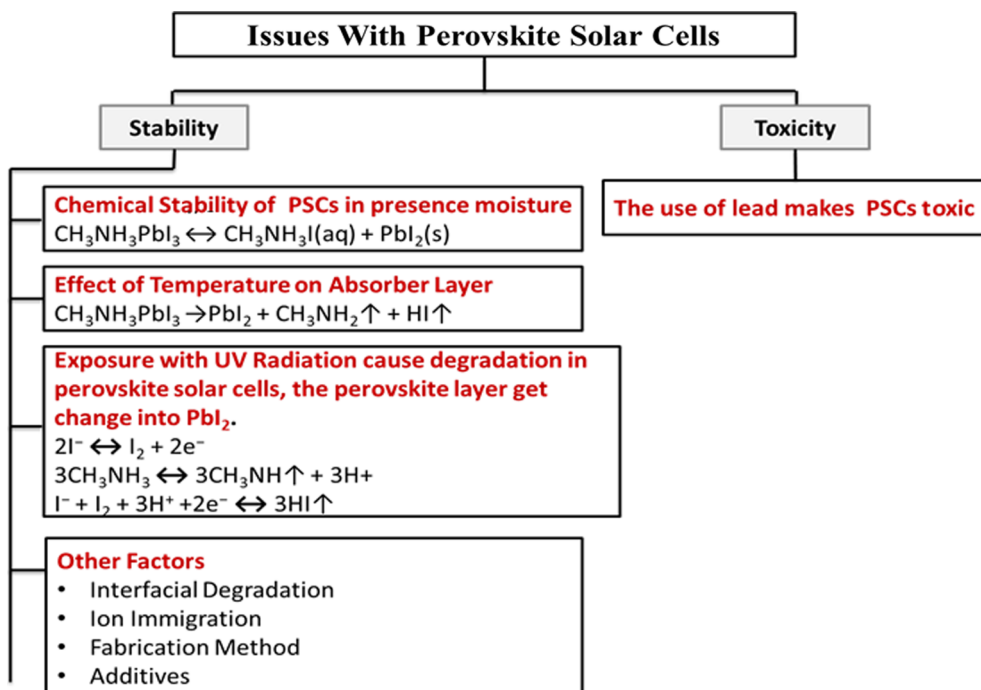
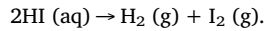
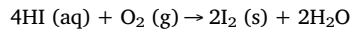
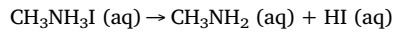
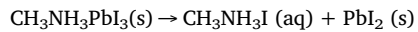


Fig. 15. Representation of commercialization issues of PSCs.

The issue of toxicity of PSCs is tackled by using Sn instead of Pb by many researchers, but Sn-based PSCs came out to be more sensitive towards moisture. Therefore for lead-free perovskite, the encapsulation becomes very important. Cavity glass and UV curable resin can be used for encapsulation (Asghar et al., 2017).



Oxygen exposure is not harmful if the device is unilluminated, as perovskite cannot be oxidized at ground state (Niu et al., 2015; Sanchez et al., 2014; Unger et al., 2014). But degradation due to oxygen is evident when perovskite film is open to illumination as the excited electrons in the conduction band become oxidized by molecular oxygen. Aristidou et al. explained the mechanism of this degradation where molecular oxygen interacts with excited electron and forms superoxide $\text{a}_{\text{ion}}\text{O}_2^-$. This further degrades the MA cation and forms CH_3NH_2 , I_2 , PbI_2 , and water (Omondi, 2018). However, the ambient atmosphere is not the only source of oxygen for degradation to take place. Jung et al. examined glass/FTO/c-TiO₂/m-TiO₂/MAPbI₃/Spiro-OMeTAD/Au using TEM and found that oxygen ion was supplied from m-TiO₂, which was diffused to perovskite film upon biasing (Joon Jung et al., 2017). Many research works have suggested that using Cl or Br along with I is beneficial for enhancing the stability of PSCs rather than using simply MAPbI₃ (Jeon et al., 2014). Alsari et al. compared the performance of $(\text{FA})_{0.83}\text{Cs}_{0.17}\text{Pb}(\text{I}_{0.8}\text{Br}_{0.2})_3$ and MAPbI_{3-x}Cl_x PSCs and obtained that MAPbI_{3-x}Cl_x collapsed very early as compared to mixed cation due to the oxygen exposure. They revealed that the oxygen-induced loss leads to a reduction in PCE due to the creation of electron traps inside the perovskite photoactive layer (Alsari et al., 2018). Improved PV performance and moisture resistant property were achieved by Li et al. by crosslinking MAPbI₃ crystals with bifunctional 4-ABPA ammonium cations. The modified cell enabling stable performance for a period greater than 1000 h and showed better performance when compared with pristine based PSC (Nazeeruddin et al., 2015). Zhou et al. improved the stability of an inverted planar PSC by using polyethylenimine (PEI) amended cross-stacked super-aligned carbon nanotube (CSCNT). The modification of CSCNT by the addition of PEI in 0.5% wt concentration caused appropriate energy level alignment and enhanced rate of interfacial charge transfer (Zhou et al., 2018). The use of proper encapsulation can protect our cell from moisture and excess oxygen or by finding a new alternative which will enhance the stability. Like benzylamine (BA) and Zractylacetones (ZrAcac) were used as isolated layers in order to increase the lifetime of PSCs in ambient air (Chen et al., 2017; Wang et al., 2016).

6.2. Temperature effect

Thermal instability is another concern of scientists for PSCs. Solar cells must possess the capability to withstand elevated temperature conditions as the operating temperature for solar cells ranges from 40 °C to 85 °C. Annealing being the necessary step for perovskite film formation shows that perovskites are likely to face high temperatures. MAPbI₃ has low thermal conductivity (Pisoni et al., 2014) and also degrades at a temperature of 85 °C even in the inert atmosphere (Conings et al., 2015). The heat-induced by irradiation cannot be easily removed making the issue due to thermal effect more deplorable for the PSCs. The organic cation component is volatile in nature and tends to degas at high temperatures (Yusoff and Nazeeruddin, 2016). Coining et al. reported that the perovskite layer decomposes into PbI₂ on heating in the nitrogenous environment at 85 °C, the complete removal of the organic component (MA). The experiment was conducted in pure dry oxygen, pure dry nitrogen, at ambient atmosphere with 50%

relative humidity in dark for 24 h (Conings et al., 2020). This fact was further confirmed by Kim et al. where they examined the thermal stability of MAPbI₃ film at three distinct temperatures: (i) room temperature (ii) 100 °C (iii) 200 °C. The hard X-ray photoelectron spectroscopy (HAXPES) the analysis was done to estimate the MAPbI₃ to PbI₂ ratio, which came out to be 85:15 to 73:30, 0:100 respectively. This further confirmed the fact that with an increase in temperature MAPbI₃ starts turning into PbI₂ (Kim et al., 2016). A stable PV cell must possess thermal stability up to 85 °C (Kim et al., 2016). The formation energy of MAPbI₃ lies in the range of 0.11–0.14 eV, which is closer to 0.093 eV. This leads to the degradation of MAPbI₃ due to continuous exposure to 85 °C (Supasai et al., 2014). The decomposing temperature of the perovskite film lies between 100 and 140 °C (Philippe et al., 2015). In order to combat the instability arising due to MA researchers used larger cation FA instead of MA. Eperon et al. studied the thermal conductivity of FAPbI₃ and MAPbI₃ film by heating them at 150 °C in an open-air condition. They noticed that MAPbI₃ film transformed into PbI₂ whereas FAPbI₃ withstood the temperature up to 60 mins (Eperon et al., 2014). The replacement of MA organic cation with FA makes the tolerance factor to reach 0.99, which has the ability to improve thermal stability. Various researchers confirm the fact that FAPbI₃ is more thermally stable than any other perovskite (Wang et al., 2019; Binek et al., 2015; Wang et al., 2016). Researchers have also used mixed cation to deal with this issue, along with the ions of Caesium and Rubidium (Hu et al., 2017).

All inorganic PSCs are also fabricated accordingly to deal with this issue. The crystal structure of CsPbI₃ attains the cubic phase upon annealing at high temperature (300 °C), whereas CsPbBr₃ can be prepared at room temperature and is structurally stable, but has a wide bandgap of 2.3 eV (Zhang et al., 2018). Beal et al. used CsPbI₂Br, and obtained better thermal stability by withstanding the high temperature of 180 °C successfully for 30mins (Beal et al., 2017). The crystal structure has an influence on the electronic properties of the material. The temperature fluctuation leads to structural instability in the perovskite material. MAPbI₃ exists in the tetragonal phase generally at room temperature. At higher temperatures, symmetry increases and crystal structure exhibits a cubic phase and at a lower temperature, the symmetry is reduced to the orthorhombic phase (Baikie et al., 2013). The PSCs based on MAPbI₃, therefore, have a little harmful effect on performance due to the lattice distortion. Snaith et al. aimed to reduce thermal degradation by replacing the organic HTL by single-walled carbon nanotube (SWNTs) and obtained remarkable results (Habisreutinger et al., 2014). Divitini et al. studied in situ degradation in PSCs due to heat, by heating it in order to check its impact on the morphology and chemical composition. They detected the mechanism responsible for degradation that leads to the structural and chemical changes, like lead and iodine immigration, which further came out to be co-related to the film synthesis condition (Divitini et al., 2016).

The commonly used HTL (Spiro-OMeTAD) is one of the reasons for thermal degradation in PSCs. Spiro-OMeTAD tends to crystallize at a higher temperature which affects the interfaces and the contact between the absorber layer and HTL. Secondly, the additive in this material namely, 4-tert-butylpyridine (TBP) has a corrosive effect on the perovskite layer (Divitini et al., 2016). Arora et al. outshined the stability of Spiro based PSC by using an inorganic hole transport layer, copper (I) thiocyanate (CuSCN). They employed a fast solvent removal method which yielded a uniform CuSCN layer enabling a faster rate of carrier collection and extraction. The PSC exhibited high thermal stability under long term heating. The device withstood 1000 h test at 60 °C under one sun illumination condition and successfully retained 95% of PCE (Arora et al., 2017). Leo et al. achieved better thermal stability when they used Zirconium oxide layer as HTL instead of using conventional organic HTL and carbon as a back electrode. The device was placed at harsh summer season in Jeddah for a week and the surprisingly stable operation was obtained (Leo, 2015). To solve this problem, inorganic HTL (Zhang et al., 2018), some additives (Zhao

et al., 2017) and HTL free PSCs are fabricated (Shi et al., 2014) and such modification has the potential to enhance the device performance as well as stability.

6.3. Light exposure effect

The occurrence of degradation due to illumination is one of the most concerning factors regarding stability as any solar cell have to undergo illumination and electrical bias in order to generate electricity. The PSCs widely use TiO_2 as an ETL but due to its bandgap of 3.2 eV and redox property, it acts as a photocatalytic material. It oxidizes certain organic materials and water also to yield OH radical (Das et al., 2018). Snaith studied degradation under UV illumination and claimed that the Titania photoanode when encapsulated in the nitrogenous atmosphere, exhibits quick decay in the PCE. He then claimed that non encapsulated PSC in an open-air condition showed better stability as it removes the surface state from titania. The degradation arises due to UV illumination which affects the titania layer. This is attributed to the light persuaded desorption of the surface-induced oxygen. They stated that as the device gets exposed to open air during processing, these deep traps get passivated because of the adsorption of oxygen. The degradation pathway under illumination is shown by the following equations:

The TiO_2 layer extracts electron and forms I^- ion and breaks the perovskite structure which leads to the formation of I_2 . However, when it comes in contact with UV rays, the desorbed oxygen from vacancy sites of oxygen and deep trap gets activated. These further increases the recombination of charge carrier within the device thereby reducing the fill factor (FF) and open-circuit voltage (V_{oc}) (Leijtens et al., 2013). To overcome this they came up with a TiO_2 free mesosuperstructured PSC. The device gave obtained a stable photocurrent upto 1000 h for continuous illumination of full-spectrum simulated sunlight. Certain research work then suggested doping the TiO_2 layer using a trivalent cation (Ga^{3+} , Nd^{3+} , Al^{3+}) and to minimize the oxygen vacancies (Roose et al., 2018; Zhu et al., 2016). Optimization of the TiO_2 must be done during its synthesis to minimize the oxygen vacancies. Snaith et al. replaced m- TiO_2 by insulating m- Al_2O_3 scaffolds and obtained better stability up to 1000hr with AM 1.5 illumination at 40 °C (Snaith, 2013). Some researchers added a UV filter to get rid of the degradation arising due to UV exposure. Wojciechowski et al. replaced the titania layer by fullerene (C_{60}) and witnessed a stable device performance even in the light soaking environment (Wojciechowski et al., 2015). Chander et al. added a UV filter before titania, they sprayed the coating of $\text{YVO}_4:\text{Eu}^{3+}$ nanophosphorous layer at the backside of the FTO glass and obtained better stability. However, using UV filters have drawbacks too, (i) reduction in the PV performance of the cell (ii) cost enhancement (iii) susceptible to photobleaching (Chander et al., 2014). A layer of Sb_2S_3 was inserted at the interface of MAPbI_3 and m- TiO_2 , it was seen that the stability of the device was enhanced with this modification (Ito et al., 2014). Tsai et al. used octithiopene-based conjugated polymer which acts as a UV filter in the inverted PSCs. The electrons generated at the perovskite absorption layer have a tendency to react with molecular oxygen and form superoxide (O_2^-). This O_2^- ion has a tendency to react with Methylammonium (MA) of the perovskite absorber layer. They advised that the rate of degradation of the perovskite layer due to oxygen and light can be reduced by using an interlayer. This interlayer poses the ability of removal of the electron which will prohibit the formation of form superoxide (O_2^-) ions. This further implied that replacing MA with a species with no acid proton will improve the tolerance towards oxygen and enhance the stability (Bryant et al., 2016). Turren-Cruz1 et al. reported that avoiding the use of MA in PSCs will substantially improve the stability of the cell. They suggested compositional engineering i.e. inorganic cation tuning by using Cs and Rb, which forms a fine crystalline formamidinium (FA)-based PSC, thereby avoiding the use of MA. Their fabricated cell attained PCE of 20.35% (highest among MA free PSC) and had enhanced stability by withstanding 1000 h illumination test (Hagfeldt and Saliba, 2018).

6.4. Other factors

Apart from moisture, oxygen, temperature, and illumination, there are some other factors too which affect the device performance of PSCs. They include additives in layers, charge selective contacts, interfaces (ETL/perovskite and HTL/perovskite), fabrication techniques and electrical biasing (Asghar et al., 2017).

The behavior of PSCs upon the application of an electrical bias is a matter of concern due to the low formation energy of Frenkel and Schottky defects and high ionic conductivity. Some theoretical studies have shown vacancy facilitated migration of FA^+ , MA^+ , I^- ions. The ions possess low activation energy in the range 0.1–0.8 eV, which is comparable to the energies of ions of the conductors (Eames et al., 2015; Azpiroz et al., 2015; Haruyama et al., 2015). At biased condition, these ions can easily accumulate and migrate at the perovskite/contact interface reducing the build-in potential and charge collection efficiency (Tress et al., 2015). The hybrid organic–inorganic perovskites exhibit ionic properties and poses low activation energy for ion migration. The rate of ionic migration increases with an increase in external electric bias, thermal stress, and illumination. The consequence of ion immigration can be explained in the following work: I^- ion when migrates through the perovskite layer and reaches the interface with perovskite layer and metal electrode. This generates defects which further act as a recombination site at the grain boundaries (Li et al., 2017). Ion immigration creates huge damage to the PSCs by contributing to the J-V hysteresis curve (Van Reenen et al., 2015; Calado et al., 2016) and creating irreversible structural damage in ambient air (Leijtens et al., 2015). Other photosensitive material like Silicon does not have the problem of ion immigration.

The interface between charge transport layers and the absorber layer plays a vital role in the proper charge collection. It is one of the performance deciding factors for any PSC. The hydrophilic nature of the perovskite layer distorts the tetragonal crystal structure and creates pinholes and irregularities at the interface of ETL/perovskite and HTL/perovskite. These irregularities may further serve as recombination centers thereby reducing the carrier charge density. To avoid this issue, Al_2O_3 was inserted in between as a buffer layer (Noh et al., 2013). The trapped charge at the interface has the ability to trigger out the moisture-induced degradation. Therefore, Ahn et al. concluded in their study that charge accumulation at the interface had to be prevented along with proper device encapsulation for the proper functioning of PSCs (Ahn et al., 2016). Xiang et al studied the interfacial degradation in PSC with configuration ITO/PEDOT: PSS/ MAPbI_3 /PCBM/Al and disclosed that the interface of MAPbI_3 and PCBM leads to degradation. They proposed a comparatively stable device by modifying the MAPbI_3 /PCBM interface by the incorporation of TiO_2 nanoparticles in it. The device worked by retaining 75% of initial PCE for about 200 h (Xiong et al., 2016). Liang Xu et al. performed a theoretical study to minimize performance degradation due to interfacial recombination in PSCs by tailoring the transport layer electronic properties like defect density, doping concentration, and electronic level positioning. They suggested choosing a transport layer with a suitable band diagram rather than passivating the interface defects in order to obtain good PCE. They further provided the guidance for proper designing of transport layers for a high PCE (Xu et al., 2018;6.). Device performance can also be improved by the modification of the film fabricating process (Liu et al., 2017). Noh et al. altered the stoichiometry of MAPbI_3 by inserting Br along with I ion and witnessed improved stability (Jeon et al., 2014). It is a well-known fact that crystal growth plays a major role in the morphology of the film. The addition of additive plays a vital role in the dynamics of crystallinity and crystal growth. Additives like fullerene, polymer, solvents, inorganic/organic halide salts, and nanoparticles are used in PSCs to raise the device performance (Li et al., 2017). Polymers are believed to promote crystal growth kinetics and acquire uniform crystallization. As polymers with good solubility in solvents possess an ability to decrease the contact angle which helps the precursor solution

to have better film coverage, better crystallinity that in turn enhances the device performance. Su et al. were first to use polyethylene glycol (PEG) as an additive in the precursor solution and effectively fabricated a high-performance device (Chang et al., 2015). Jin et al. used $ZnCl_2$ along with PbI_2 while fabricating $MAPbI_3$ film, and obtained efficiency increment by 2% with a comparatively better lifetime (Jin et al., 2017). The instability in PSCs is also attributed due to the grain boundaries by some researchers (Nazeeruddin et al., 2015; Ran et al., 2018; Ahn et al., 2016; Zheng et al., 2017; Wang et al., 2017). By the means of capping of these grain boundaries with certain protective material, one can improve the stability. Li et al. used tetra-ammonium zinc phthalocyanine ($ZnPc$) to post-treat the $MAPbI_3$ film. This led to the formation of $(ZnPc)_{0.5}MA_{n-1}Pb_nI_{3n+1}$ between the grain boundaries of the $MAPbI_3$ film, thereby passivating the defects within the grain boundaries. The results of time-resolved photoluminescence indicated the minimization of trap assisted recombination loss as decay time increased from 44 ns to 57 ns. The device also exhibited enhanced device stability by losing only 10% of the initial PCE after 1000 h (Cao et al., 2018). Steele et al. reported a way to stabilize the material Cesium lead triiodide ($CsPbI_3$) and to make it a good solar absorber. $CsPbI_3$ is one of the promising materials for PV application but is highly unstable. Generally, at room temperature, these crystals being yellow in colour hardly form perovskite structure. In order to turn them black for better absorption, they binded the thin film of PSC with a glass sheet. The film was annealed at 330 °C for better expansion and adhesion into the glass (Steele et al., 2019). This modification made $CsPbI_3$ be stable at room temperature and retain its black color. The enhancement in the PCE was seen in PSC by the addition of Bidentate (Bpy) and tridentate (Tpy) additive, whereas the unsatisfactory result was obtained on the addition of monodendate pyridine (py). Bidentate (Bpy) and tridentate (Tpy) as additives elongated the carrier lifetime and raised the grain size (Chen et al., 2019). Therefore, all such works suggested the fact that the selection of proper additives and proper processing of material might enhance device performance and stability, whereas improper selection of additive may also degrade it. Huang et al. successfully avoided the loss of photon energy inside the PSC by modulating the path of light within the cell. They used four horizontally connected cell of varying bandgap (typically $MAPbBr_3$, $MAPbI_2Br$, $MAPbI_2Br$, $MAPbI_3$ was used as absorber layer). The cells had the configuration of indium tin oxide (ITO)/NiO/ $MAPbI_{3-x}Br_x$ ($x = 0, 1, 2$ or 3)/electron transporting layer (ETL) (ICBA, PCBM or ICBA:PCBM)/Al. The incident light initially falls at cell-1, here the high energy incident photons were initially absorbed by $MAPbBr_3$ active layer cell. Then the photons were reflected by the cell-2 opposite reflector and further get absorbed by $MAPbI_2Br$ active layer cell. In the similar way, the incident light gets absorbed by the other two cells, shown in Fig. 16.

This modification gave the highest record open-circuit voltage (V_{oc}) of 5.3 V and PCE of 21.3%. This modification is equally applicable to large area cells and also to flexible modules (Huang et al., 2019). Grancini et al. reported an ultra-stable PSC with the help of interface engineering. They created 2D/3D perovskite junction ($HOOC(CH_2)_4NH_3^+$) $2PbI_4/CH_3NH_3PbI_3$ and fabricated HTM free modules and PSCs, using carbon electrode. An efficiency of 12.9% and 14.6% was attained in carbon-based and mesoporous architecture respectively. The large scale production ability was also explored by using a fully printable industrial-scale technique. A solar module of dimension 10x10cm was fabricated with high efficiency of 11.2%. The PSC exhibited stable performance for more than 400 days with zero percentage reduction in the efficiency. These groups of researchers formed a fully printed, low cost and efficient PV module with an active area of 50 cm^2 and module area of 100 cm^2 in presence of moisture and oxygen and in a controlled environment. They claimed that the 2D perovskite remained protected against moisture by acting as a protective window, thereby conserving the 3D perovskites which further contributed to the device stability (Grancini et al., 2017). The device performance along with the stability of the fabricated cell and module is shown in Figs. 17 and 18.

6.5. Toxicity

It is a well-known fact that toxicity due to lead (Pb) can cause severe health risks and also has a deplorable impact on our ecosystem. This is one of the factors, creating a negative impact on users and avoiding its market acceptance of the final product. In order to avoid this issue, two types of corrective measure have been applied till date by 1) Forming a low toxic metal cation by partially replacing lead with another low toxic metal; 2) Completely omitting lead and using other metals like Sn^{2+} , Sn^{4+} , Ge^{2+} , Cu^{2+} , Bi^{3+} and Sb^{3+} (Lyu et al., 2017). Here, it is important to mention that the PSCs with full replacement of toxic Pb have the highest reported efficiency upto 9%. (Shao et al., 2018).

The incorporation of tin (Sn) along with lead was first done by Ogomi et al. in 2014, they used $CH_3NH_3Sn_{0.5}Pb_{0.5}I_3$ as the absorber layer and the device attained an efficiency of 4.18%. The cell was able to harvest light up to the wavelength of 1060 nm. Thus suggested the fact that Sn/Pb based solar cells could act as an efficient bottom solar cell in tandem architecture (Ogomi et al., 2014). Later Hao et al. raised the efficiency to 7% by replacing the HTL material with 2,2',7,7'-tetraakis(N,N-di-pmethoxyphenylamine)9,9'-spirobifluorene (spiro-OMe-TAD) (Hao et al., 2014). The Sn-based PSCs are stated to have a narrow band-gap ($E_g \sim 1\text{ eV}$) and much higher charge mobility ($10^2\text{--}10^3\text{ cm}^2/\text{Vs}$) as compared to pure Pb-based PSCs ($10\text{--}10^2\text{ cm}^2/\text{Vs}$) (Stoumpos et al., 2013). Fan Zuo et al. raised the PCE to 10.1% by incorporating chlorine in the perovskite film to form $CH_3NH_3Sn_xPb_{1-x}I_{3-x}Cl_x$ which rendered perovskite film with a larger crystal grain size (500 nm). The high efficiency was attained due to the reduction in the interfacial and internal resistances (Zuo et al., 2014). Later the PCE was further increased to 14.35% for $CH_3NH_3Sn_{0.25}Pb_{0.75}I_3$ with an identical device configuration (Yang et al., 2016). Some other low toxic metal Cations like Mn^{2+} , Ge^{2+} , Co^{2+} , Al^{3+} , In^{3+} , and Sb^{3+} are alloyed with lead-based perovskite to tackle the toxicity issue. Several attempts were made to conquer the toxicity issue, but still PCE comparable to lead halide based PSCs are not achieved. Rohan Mishra and co-workers reported an inorganic, lead-free, and double perovskite material ($KBaTeBiO_6$) for PV application. This material not only exhibited a favourable bandgap of 1.88 eV but also have a comparable effective mass for a charge carrier to the prototype bismuth halide double perovskite. $KBaTeBiO_6$ nanoparticles based PSC exhibited PCE of 0.057% (Thind et al., 2019). Shin et al. reported Cs_2SnI_6 (vacancy-ordered double perovskite) to be a promising candidate for optoelectronic applications. They came up with dye-sensitized Cs_2SnI_6 solar cell with configuration fluorine-doped tin oxide (FTO)/dyed mesoporous TiO₂/regenerator/poly(3,4-ethylene dioxythiophene)/FTO. The device achieved 79% increment in photocurrent density (14.1 mA/cm^2) as compared to conventional liquid electrolyte based solar cell (7.9 mA/cm^2) (Shin et al., 2019). Among all the attempts to lead-free PSCs, Sn-based PSCs seems to be the potential candidate for attaining high performance. However, even with proper encapsulation, the Sn-based PSCs still has lower stability as compared to Pb-based PSCs. The Ge-based PSCs have exhibited poor device performance, although by using Ge/Sn-based PSCs efficiency higher than 10% can be attained. Unfortunately, Sn-based PSCs did not gain much attention due to the easy oxidation of Sn^{2+} to Sn^{4+} . To date, the Pb-free materials used in PSCs exhibits irreconcilable different behaviour: (i) stable but low efficiency (Sn^{4+} based), (ii) efficient but low stability (Sn^{2+} based) (Chen et al., 2019). To replace Pb-based material, the new candidate must exhibit good performance along with proper stability, compatible with scalable fabrication techniques and should be low cost.

PSCs are not the only solar cell which contains the incorporation of toxic elements within it. The other toxic elements widely used in PV panels include copper indium selenide, cadmium telluride, copper indium gallium (di) selenide, cadmium gallium (di) selenide, hexa-fluoroethane, and polyvinyl fluoride. Also, silicon tetrachloride, which is a byproduct during the production of crystalline silicon is highly venomous. Moreover, the amount of lead used in PSCs is very less as

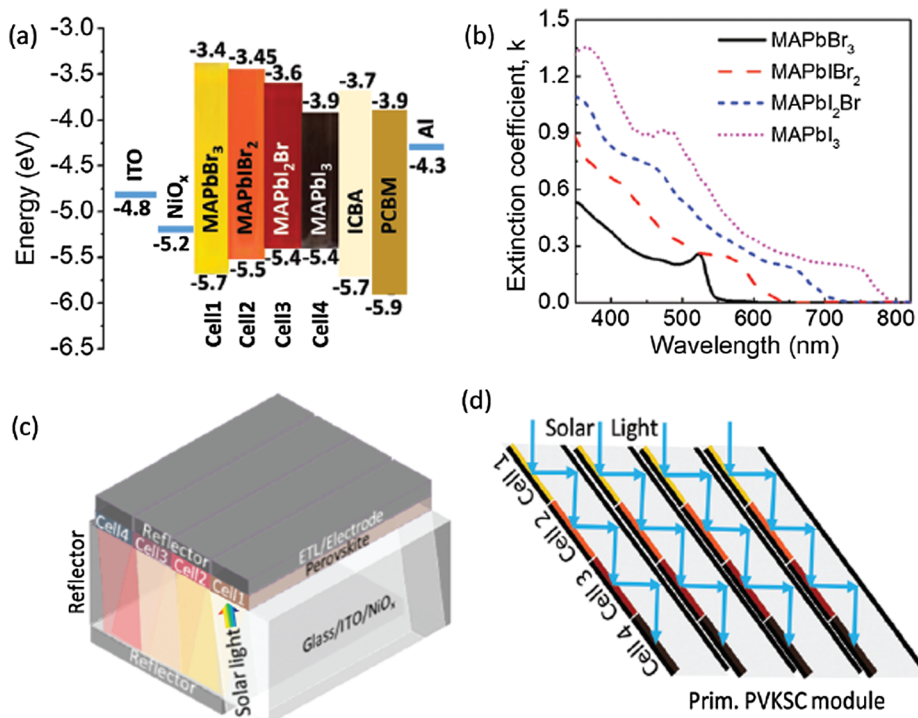


Fig. 16. Energy diagrams, light absorption spectra of active materials and device structures in this work. (a) Energy level diagrams of PVK solar cells; (b) extinction coefficients of PVK films including MAPbBr₃, MAPbIBr₂, MAPbI₂Br, and MAPbI₃. (c) Device configuration of Prim PVSC including 4 subcells. (d) Prim PVSC module structure with the path of solar light. Reprinted with permission from Ref. (Huang et al., 2019). Copyright (2019) RSC Publishing.

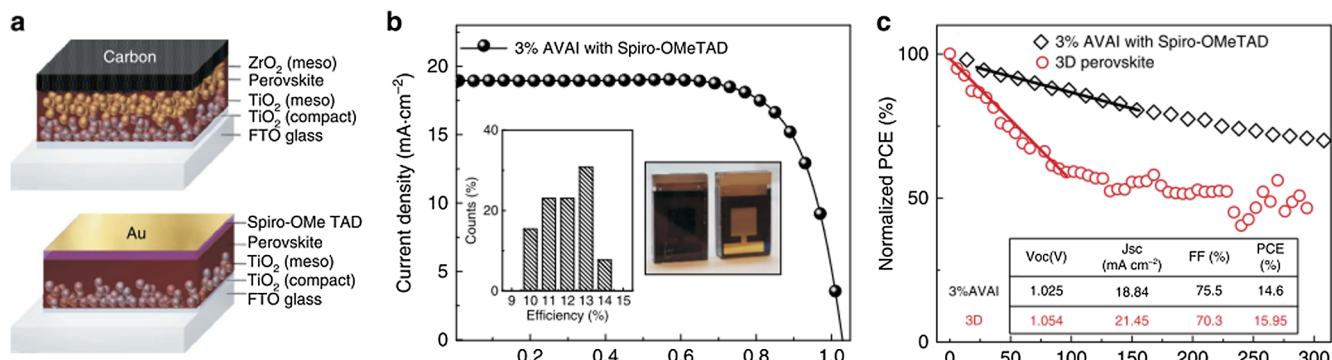


Fig. 17. 2D/3D Mesoporous Solar cell characteristics and stability. (a) Device cartoon of the Hole transporting Material (HTM)-free solar cell and of the standard HTM-based solar cell. (b) Current density voltage (J-V) curve using the 2D/3D perovskite with 3% HOOCC(CH₂)₄NH₃I, AVAI hereafter, in a standard mesoporous configuration using 2,20,7,70-tetrakis(N,N-di-p-methoxyphenylamine)-9,90-spirobifluorene (spiro-OMeTAD)/Au (device statistics and picture of the cell in the inset). (c) Stability curve of the Spiro-OMeTAD/Au cell comparing standard 3D with the mixed 2D/3D perovskite at maximum power point under AM 1.5G illumination, argon atmosphere and stabilized temperature of 45 °C. The solid line represents the linear fit. In the inset the champion device parameters are listed. Reprinted with permission from Ref. (Grancini et al., 2017). Copyright (2017) Nature Communications.

compared to lead used in other widely adopted devices like lead-cadmium batteries, integrated circuits, infrared detectors, etc. The above-stated fact is supported by Nam-Gyu Park et al., where they stated that only 0.4 g/m² of Pb was being used in PSCs, which is comparatively much smaller than the lead used in soldering of commercial Si PV panels (Chen et al., 2019). It is also the well evident fact that lead-free PSCs are still lagging behind in performance as compared to lead-based PSCs. In comparison to all the commercialization issues, firstly the main emphasis must be laid on the improvement of the device instability issue in Pb-based PSCs. The device performance of some of the low-lead perovskite solar cell is shown in Table 4.

7. Commercialization status

There are three deciding factors for commercialization of a solar cell, (i) device performance (ii) cost (iii) stability. The advancement in the device architecture and fabrication processes, which raised the device performance have led the commercialization of PSCs to an

unstoppable trend. Now PSCs have started stepping out from laboratories to the commercial markets. The PSCs possess better device performance and impressively low production costs. The device stability has been a matter of issue for researchers and industries. However, PSC which is stable up to a year is already achieved (Mei et al., 2014; Grancini et al., 2017). Many initiatives are being taken by certain promising companies with an aim to launch PSCs in the market. To date, PSCs with high efficiency could be fabricated mostly with a small-sized device (0.03–0.2 cm²), which is too small for commercialization (Huang et al., 2018). The most important industry standard for a PV cell is given by International Electrochemical Commissions (IEC) as an IEC 61215 norm. It comprises a series of detailed, time consuming and interrelated stress tests. Approval from this test is a minimum and important requirement for winning the confidence of consumers and investors which leads to commercialization. Through this test one may depict the information regarding long term stability and performance of solar modules. Holzhey et al. reported the most current stability standard IE- 61215 test is passed by the PSCs. Although PSCs have seemed

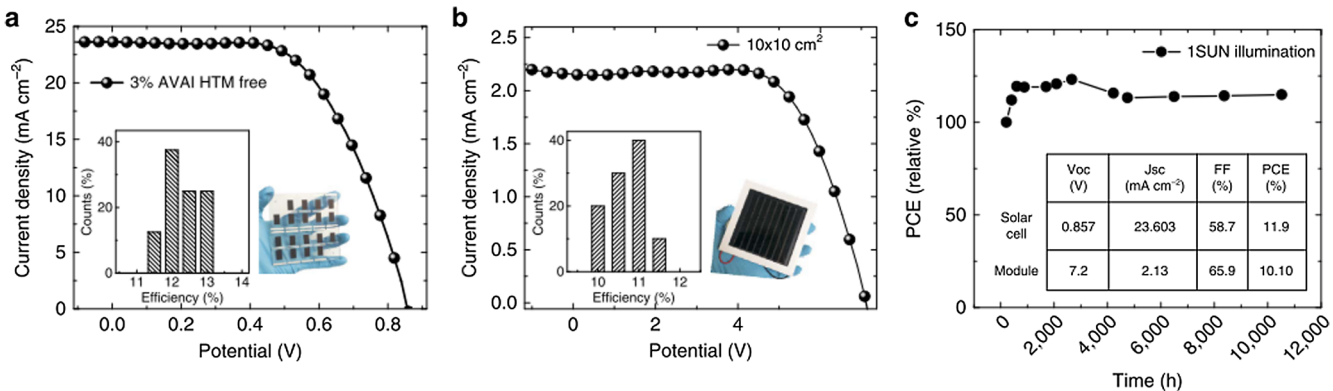


Fig. 18. 2D/3D Carbon-based Solar cell characteristics and stability. (a) J-V curve using the 2D/3D perovskite with 3%AVAI in HTM-free solar cell measured under Air Mass (AM) 1.5G illumination (device statistics and picture in the inset). (b) J-V curve using the 2D/3D perovskite with 3%AVAI in an HTM-free 10 \times 10 cm 2 module (device statistics and picture in the inset). (c) Typical module stability test under 1 sun AM 1.5 G conditions at stabilized temperature of 55° and at short circuit conditions. Stability measurements were done according to the standard aging conditions. In the inset device parameters of the devices represented in a and b. Champions. Reprinted with permission from Ref. (Grancini et al., 2017). Copyright (2017) Nature Communications.

Table 4
Device performance of some the low-lead perovskite solar cell.

PCE (%)	V _{oc} (v)	J _{sc} (mA/cm ²)	FF	Device configuration	Year	Reference
10.2	0.72	19.2	0.73	FTO/TiO ₂ /N719 Dye/Perovskite/ZnO	2012	(Chung et al., 2012)
2.02	0.24	22.7	0.37	FTO/Compact TiO ₂ /Mesoporous TiO ₂ /Perovskite/m-MTADATA /Au	2014	(Kumar et al., 2014)
4.63	0.57	13.2	0.61	FTO/TiO ₂ / Dye/ Cs ₂ SnI ₆ + Z907/Pt	2014	(Lee et al., 2014)
6.32	0.63	14.7	0.68	FTO/TiO ₂ / Dye/ Cs ₂ SnI ₆ + N719/Pt		
6.94	0.62	16.9	0.66	FTO/TiO ₂ / Dye/ Cs ₂ SnI ₆ + multiple/Pt		
7.8	0.62	18.6	0.68	FTO/TiO ₂ / Dye/ Cs ₂ SnI ₆ +(with 3D Phc)/Pt		
7.37	0.73	15.8	0.64	Au/TiO ₂ /m-TiO ₂ /MASn _{0.25} Pb _{0.75} /Spiro-OMeTAD/Au	2014	(Hao et al., 2014)
6.4	0.88	16.8	0.42	TiO ₂ /m-TiO ₂ /MASnI ₃ /SpiroOMeTAD + LiTFSI + tBP/Au	2014	(Noel et al., 2014)
9.8	0.76	19.1	0.66	ITO/PEDOT:PSS/MAPb _{0.85} Sn _{0.15} I _{3-y} Cl _y /PC ₆₁ BM/Ag	2014	(Zuo et al., 2014)
7.66	0.97	11.1	7.66	ITO/ZnO/MASnI ₃ /spiro-OMeTAD/Au	2015	(Bansode et al., 2015)
10.2	0.7	21.9	0.66	ITO/PEDOT:PSS/FASn _{0.5} Pb _{0.5} I ₃ /C ₆₀ BCP/Ag	2016	(Eperon et al., 2016)
14.1	0.74	26.1	0.71	ITO/PEDOT:PSS//C ₆₀ BCP/Ag		
14.06	0.79	22.8	0.78	ITO/PEDOTPSS/MA _{0.5} FA _{0.5} Pb _{0.75} Sn _{0.25} I ₃ /PC ₆₁ BM/C ₆₀ /Ag	2016	(Yang et al., 2016)
15.08	0.79	26.86	0.70	ITO/PEDOT:PSS/(CH3NH3) _{0.4} [HC(NH ₂) ₂] _{0.6} Sn _{0.6} Pb _{0.4} I ₃ /C ₆₀ /BCP/Ag	2016	(Liao et al., 2016)
17.55	1.03	21.9	0.78	ITO/PEDOT:PSS/MAPb _{0.85} Sn _{0.15} I ₃ Cl _{0.15} /PC ₆₁ BM/ Bphen/Ag	2016	(Wang et al., 2016)
19.1	1.01	22.4	0.78	FTO/Poly-TPD/0.15 mol% Al3+ -doped CH3NH3PbI3/PCBM/BCP/Ag	2016	(Ramirez et al., 2016)
9	0.52	24.1	0.71	ITO/PEDOT:PSS/FA SnI ₃ /C ₆₀ BCP/Ag	2017	(Shao et al., 2017)
12.1	0.78	20.65	0.75	ITO/PEDOT: PSS/MASn _{0.6} Pb _{0.4} I _{3-x} Br _x /PCBM/Ag	2017	(Lee and Kang, 2017)
9.2	0.61	21.2	0.72	ITO/PEDOT:PSS/ GA _x FA _{0.98-x} SnI ₃₋₁ -EDAI ₂ (20 nm)/BCP/Ag	2018	(Jokar et al., 2019)
6.7	0.6	17.53	0.65	ITO/NiO _x /FASnI ₃ /PCBM/Ag	2018	(Tai et al., 2019)
4.2	0.55	13.1	0.58	(FTO)/D-DAHTDTT m-TiO ₂ /Cs ₂ SnI ₆ / poly(3,4-ethylenedioxythiophene)/FTO		
7.0	0.71	13.5	0.71	(FTO)/ T-DAHDTDTm-TiO ₂ /Cs ₂ SnI ₆ / poly(3,4-ethylenedioxythiophene)/FTO		
4.3	0.61	9.9	0.73	(FTO)/ BT-Tm-TiO ₂ /Liquid electrolyte/ poly(3,4-ethylenedioxythiophene)/FTO		
6.1	0.62	14	0.7	(FTO)/ BT-HT-TiO ₂ / Cs ₂ SnI ₆ / poly(3,4-ethylenedioxythiophene)/FTO	2018	(Shin et al., 2019)

to pass IEC-61215 in order to appropriately predict the long term stability of PSC modules more points must be taken into consideration like its mechanical stability, humidity freeze stability, high voltage and reverse bias (which is related to hotspot damage) (Holzhey and Saliba, 2018).

The current aim of the researchers and PV industries is to advance and modify manufacturing processes to fabricate large-area devices (1 cm² or greater) while maintaining the same efficiency as achieved in the case of small area devices along with good stability (Huang et al., 2018). Now the deciding factor for commercialization is moved from obtaining better device performance to stability, device upscaling, reproducibility, and avoiding leakage of Pb from module during device working lifetime. Yan Jiang et al. came up with an alternative to avoid Pb leakage by using encapsulation by epoxy resins instead of conventional glass encapsulation. They simulated this data in realistic conditions and analyzed PSC modules with different encapsulation techniques. They mechanically smashed encapsulations by hail impact (modified FM 44787 standard) and reported that the reduction of the Pb leakage rate decreased by a factor of 375 in comparison to the encapsulation technique based upon glass cover with a UV cured resin

(Jiang et al., 2019).

In 2016, Solaronix, a Switzerland based the company came up with its high performance and stable all print 500 cm² perovskite module with 12% efficiency (Solaronix Achieves Major Breakthrough Toward Perovskite Solar Cell Industrialization, 2016). In 2017, they fabricated a low cost and stable PSC and were successful to raise the efficiency to 14% using carbon-based monolithic PSCs at the lab scale. The as-fabricated PV module was resistant towards damp and heat, which indicated that such modification, could be beneficial in the case of non-encapsulated devices. The device was in working for 10,000 h with the similar performance (Sarikka and Ulla, 2017; Continuing Progress in Perovskite Industrialization, 2017). Later, in 2017, Gratzel group, Solaronix, and EPFL collaborated and produced the fully printed 100 cm² PV panels with a PCE of 11.2% that was stable over a year. In December 2018, Oxford PV, the perovskite company announced the efficiency of their champion 1 cm² perovskite-silicon tandem cell to attain the highest PCE as 28% beating their own previously attained highest PCE of 27.3%. This achievement was appreciated and certified by NREL. Dr. Chris Case, the Chief Technology Officer at Oxford PV said that they will continue to raise the bar and achieve the efficiency of perovskite-

Table 5

Details of companies producing PSCs and their recent advances.

Company name	Country	PCE	Cell details	Module area
Oxford photovoltaics	United Kingdom	28%	Silicon-perovskite tandem cell	1 cm ² per cell
EPFL	Switzerland	11.2%	Perovskite solar cell	100 cm ² module
OIST's Technology	Japan	20%	Perovskite solar cell (using SnO ₂ as ETL)	25 cm ² (comprises multiple cells)
Imec	Belgium	12.4%	Perovskite solar cell	16 cm ² Module
Toshiba and NEDO	Japan	11.7%	Perovskite solar cell (adjusting crystal growth)	703 cm ² Module
Solliance	Netherlands	14.5%	Using the slot die coating	144 cm ² per cell
Microquanta	China	14.24%	Perovskite solar cell	160000 cm ² Module

silicon tandem cell beyond 30%. They further claimed that the PSCs being fabricated by them are not only efficient but also stable, and all the manufactured cells have passed 2000 h heat damp reliability tests in line with IEC 61215 protocol. Although, PSCs have seemed to pass IEC 61215 in order to appropriately predict the long term stability of PSC modules more points like its mechanical stability, humidity freeze stability, high voltage and reverse bias (which is related to hotspot damage) must be taken into consideration (Oxford, 2018).

The Oxford PV entered into a partnership with the Meyer Burger, the leading photovoltaic equipment supplier to jointly raise the bulk production technology for perovskite in silicon heterojunction (HJT) tandem PV cell. They are now planning to sell their 200 MW HJT lines for pilot production of tandem cells to be installed at Brandenburg an der Havel in Germany by the end of 2020 (Oxford, 2019). Recently, Meyer Burger Technology Ltd, reported that its first order from oxford PV has been delivered, for the HJT manufacturing line comprising all essential adaption to upgrade Perovskite-on-HJT tandem technology. Details of companies producing PSCs and their recent advances are enclosed in Table 5 (Tai et al., 2019; Holzhey and Saliba, 2018).

Solliance, a well-established PV company from The Netherland has announced a new record of stabilized large perovskite thin-film module on glass with a cell performance of 14.5%. The PSC is fabricated by the application of the slot die coating process and the corresponding PCE is measured on an aperture area of 144 cm² (Dyesol secures \$1 million grant for perovskite PV research, 2016). Imec and Solliance manufactured a perovskite PV module with an area of 4x4 cm² and a certified efficiency of 12.4% (IMEC AND SOLLIANCE'S PEROVSKITE PV MODULES ACHIEVE, 2017). Solliance, in order to achieve large scale manufacturing of flexible PSCs, collaborated with Panasonic for the development of roll to roll manufacturing processes (PANASONIC JOINS SOLLIANCE AS AN INDUSTRIAL PARTNER, 2019). Toshiba and New Energy and Industrial Technology Development Organization (NEDO) fabricated a module with bigger dimensions of 703 cm² (24.15 × 29.10 cm), thereby overcoming the issue of large size with good efficiency. They controlled the crystal properties during the crystal growth process during fabrication via printing (Toshiba Develops, 2018). In a recent development, China-based Perovskite making company, Microquanta successfully fabricated a large area cell (200x800cm² per module) with PCE of 14.24% (Microquanta achieves 14.24% efficiency with large-area perovskite solar module, 2019). Recently, Okinawa Institute of Science and Technology Graduate University (OIST) solved the problem of low stability and scalability of perovskite solar cells by replacing one of the unstable component (TiO₂) by tin dioxide (SnO₂) and attained enhanced lifetime, which is expected to contribute to the commercialization of PSCs (Qiu et al., 2018). Great cell, formerly known as Dyesol put forward its roadmap for commercialization of PSCs and came up to launch a prototype in 2018. Unfortunately, in December 2018, Dyseol was declared bankrupt. Prior to this bankruptcy (in September 2018), Greatcell Solar sold their Production Division, in a new business entitled Greatcell Solar Materials (GSM), where they supplied perovskite precursors, various dopants, silver inks, etc. to the research community. This company is presently supplying all the materials required for the production of PSCs, which will be beneficial for early level researchers (GreatCell

unveils its perovskite-based solar cells commercialization roadmap, 2018; Interview with Greatcell Solar Materials' GM Yanek Hebing, 2019). Saule Technologies have been able to print PSCs with light-weight, flexible and semi-transparent single-junction PV modules with 10% efficiency. They are about to expand their line printing capacity from 40,000 m²/annum to 200,000 m²/annum. Recently, Saule Technologies signed a cooperation agreement with Skanska commercial business unit. These two firms aim to cover office buildings with PSCs over commercial scale (Saule Technologies' perovskite-based solar panels headed for commercial implementation by building company Skanska, 2018; Saule Technologies, 2019). Saule Technologies have installed PSC modules in an innovative Japanese Hotel, named Henn-na. The installed commercial prototype had 72 PSC modules, which are encapsulated inside a curved glass (Saule Technologies, 2018). The leveled cost of energy (LCOE) for perovskite module is estimated to be 4.84 to 7.90¢ per KW per hour (in US) considering the rate of degradation to be 0.5% per year (Qian et al., 2019). The LCOE of c-Si PV module is estimated to be 2.21 USD/W (The International Renewable Energy Agency, 2012). Therefore, using PSCs in place of other solar cells is more advantageous.

The enormous potentials of PSCs are encouraging many companies and government organizations to invest in this field. To promote PSC related work, the National science foundation has granted \$4 million to Brown University. The idea behind such an initiative is to develop a better understanding of the physics of PSCs and to look for more productive and scalable techniques so that PSCs can be brought to the market (Brown University to lead \$4 million solar cell research grant, 2015). U.S. Department of Energy (DoE) has provided funding of \$130 million for upgrading early-stage solar technologies (Funding Opportunity Announcement: Solar Energy Technologies Office Fiscal Year, 2019). Dyesol has announced a \$1Million grant for perovskite photovoltaic research (Dyesol secures \$1 million grant for perovskite PV research, 2016) and much more. The details of some of the PSCs producing companies with their recent advances are shown in Table 4. Other prominent players in PSC market aiming for their commercialization are Xeger Sweden AB, Alta Devices, G24 Power Ltd, FlexLink Systems, Polyera Corporation Solar Print Ltd, New Energy Technologies Inc, Korver Corp., Toshiba, Microquanta Semiconductor, Solar-Tectic, Ubiquitous Energy Inc., Saule Technologies, Fraunhofer ISE, Raynergy Tek Incorporation, Xiamen Weihua Solar Co. Ltd and few more (Perovskite companies: the comprehensive list, 2018).

Declaration of Competing Interest

The authors declare that they have no known financial interests or personal relationship that could have appeared to influence the work in this paper.

Acknowledgements

The authors are thankful to the publishers (AIP, Wiley Online, Hindawi, ACS, RSC, Elsevier, IEEE, AAAS and MDPI) of original papers for permitting reproduction of their contents.

References

- Aharon, S., Dymshits, A., Rotem, A., Etgar, L., 2015. Temperature dependence of hole conductor free formamidinium lead iodide perovskite based solar cells. *J. Mater. Chem. A* 3, 9171–9178. <https://doi.org/10.1039/c4ta05149a>.
- Ahn, N., Kwak, K., Jang, M.S., Yoon, H., Lee, B.Y., Lee, J.K., et al., 2016. Trapped charge-driven degradation of perovskite solar cells. *Nat. Commun.* 7, 1–49. <https://doi.org/10.1038/ncomms13422>.
- Alsari, M., Pearson, A.J., Wang, J.T.W., Wang, Z., Montisci, A., Greenham, N.C., et al., 2018. Degradation kinetics of inverted perovskite solar cells. *Sci. Rep.* 8, 1–8. <https://doi.org/10.1038/s41598-018-24436-6>.
- Arora, N., Dar, M.I., Hinderhofer, A., Pellet, N., Schreiber, F., Zakeeruddin, S.M., Grätzel, M., 2017. Perovskite solar cells with CuSCN hole extraction layers yield stabilized efficiencies greater than 20%. *Science* (80-) 358, 768–771. <https://doi.org/10.1126/science.aam5655>.
- Asghar, M.I., Zhang, J., Wang, H., Lund, P.D., 2017. Device stability of perovskite solar cells – A review. *Renew. Sustain. Energy Rev.* 77, 131–146. <https://doi.org/10.1016/j.rser.2017.04.003>.
- Azpiroz, J.M., Mosconi, E., Bisquert, J., De Angelis, F., 2015. Defect migration in methylammonium lead iodide and its role in perovskite solar cell operation. *Energy Environ. Sci.* 8, 2118–2127. <https://doi.org/10.1039/c5ee01265a>.
- Back, H., Kim, J., Kim, G., Kyun Kim, T., Kang, H., Kong, J., et al., 2016. Interfacial modification of hole transport layers for efficient large-area perovskite solar cells achieved via blade-coating. *Sol. Energy Mater. Sol. Cells* 144, 309–315. <https://doi.org/10.1016/j.solmat.2015.09.018>.
- Bai, Y., Fang, Y., Deng, Y., Wang, Q., Zhao, J., Zheng, X., Zhang, Y., Huang, J., 2016. Low temperature solution-processed Sb_xSnO₂ nanocrystals for efficient planar perovskite solar cells. *ChemSusChem* 9, 2686–2691. <https://doi.org/10.1002/cssc.201600944>.
- Baikie, T., Fang, Y., Kadro, J.M., Schreyer, M., Wei, F., Mhaisalkar, S.G., et al., 2013. Synthesis and crystal chemistry of the hybrid perovskite (CH₃NH₃)PbI₃ for solid-state sensitised solar cell applications. *J. Mater. Chem. A* 1, 5628. <https://doi.org/10.1039/c3ta10518k>.
- Ball, J.M., Lee, M.M., Hey, A., Snaith, H.J., 2013. *Environ. Sci.* 1739–1743. <https://doi.org/10.1039/c3ee40810h>.
- Bansode, U., Naphade, R., Game, O., Agarkar, S., Ogale, S., 2015. Hybrid perovskite films by a new variant of pulsed excimer laser deposition: a roomerature dry process. *J. Phys. Chem. C* 119, 9177–9185. <https://doi.org/10.1021/acs.jpcc.5b02561>.
- Barrows, A.T., Pearson, A.J., Kwak, C.K., Dunbar, A.D.F., Buckley, A.R., Lidzey, D.G., 2014. Efficient planar heterojunction mixed-halide perovskite solar cells deposited via spray-deposition. *Energy Environ. Sci.* 7, 2944–2950. <https://doi.org/10.1039/c4ee01546k>.
- Beal, R.E., Slotcavage, D.J., Leijtens, T., Bowring, A.R., Belisle, R.A., Nguyen, W.H., et al., 2017. Fully inorganic cesium lead halide perovskites with improved stability for tandem solar cells. In: 2017 IEEE 44th Photovolt Spec Conf PVSC 2017, pp. 1–4. doi:10.1109/PVSC.2017.8366206.
- Best Research-Cell Efficiency Chart, 2019. <https://www.nrel.gov/pv/cell-efficiency.html> (accessed March 23, 2019).
- Bi, D., Yi, C., Luo, J., Décoppet, J.D., Zhang, F., Zakeeruddin, S.M., Li, X., Hagfeldt, A., Grätzel, M., 2016. Polymer-templated nucleation and crystal growth of perovskite films for solar cells with efficiency greater than 21%. *Nat. Energy* 1, 1–5. <https://doi.org/10.1038/nenergy.2016.142>.
- Bi, D., Tress, W., Dar, M.I., Gao, P., Luo, J., Rennvier, C., et al., 2016. ACSMs Guidelines 10th Ed 2017 Chp 3 Preexercise Evaluation.pdf, doi:10.1126/sciadv.1501170.
- Binek, A., Hanusch, F.C., Docampo, P., Bein, T., 2015. Stabilization of the trigonal high-temperature phase of formamidinium lead iodide. *J. Phys. Chem. Lett.* 6, 1249–1253. <https://doi.org/10.1021/acs.jpclett.5b00380>.
- Bishop, J., Routledge, T., Lidzey, D.G., 2018. Advances in spray-cast perovskite solar cells advances in spray-cast perovskite solar cells, doi:10.1021/acs.jpclett.8b00311.
- Bonabi Naghadeh, S., Luo, B., Abdelfageed, G., Pu, Y.C., Zhang, C., Zhang, J.Z., 2018. Photophysical properties and improved stability of organic-inorganic perovskite by surface passivation. *J. Phys. Chem. C* 122, 15799–15818. <https://doi.org/10.1021/acs.jpcc.8b03681>.
- Brown University to lead \$4 million solar cell research grant, 2015. <https://www.perovskite-info.com/brown-university-lead-4-million-solar-cell-research-grant> (accessed October 7, 2018).
- Bryant, D., Aristidou, N., Pont, S., Sanchez-molina, I., Chotchunangatchaval, T., Wheeler, S., et al., 2016. Environmental Science Light and oxygen induced degradation limits the operational stability of methylammonium lead triiodide perovskite solar cells †. *Energy Environ. Sci.* <https://doi.org/10.1039/C6EE00409A>.
- Burschka, Julian, Pellet, Norman, Moon, Soo-Jin, Humphry-Baker, Robin, Gao, Peng, Nazeeruddin, Mohammad K., Grätzel, Michael, 2013. Sequential deposition as a route to high-performance perovskite-sensitized solar cells. *Nature* 499 (7458), 316–319. <https://doi.org/10.1038/nature12340>.
- Calado, P., Telford, A.M., Bryant, D., Li, X., Nelson, J., O'Regan, B.C., et al., 2016. Evidence for ion migration in hybrid perovskite solar cells with minimal hysteresis. *Nat. Commun.* 7, 1–10. <https://doi.org/10.1038/ncomms13831>.
- Cao, J., Li, C., Lv, X., Feng, X., Meng, R., Wu, Y., et al., 2018. Efficient grain boundary suture by low-cost tetra-ammonium zinc phthalocyanine for stable perovskite solar cells with expanded photoresponse. *J. Am. Chem. Soc.* 140, 11577–11580. <https://doi.org/10.1021/jacs.8b07025>.
- Zhang, Y., Zhang, H., Zhang, X., Wei, L., Zhang, B., Sun, Y., Hai, G., Li, Y., 2018. Major impediment to highly efficient, stable and low-cost perovskite solar cells. *Metals (Basel)* 8, 1–33. <https://doi.org/10.3390/met8110964>.
- Chander, N., Khan, A.F., Chandrasekhar, P.S., Thouti, E., Swami, S.K., Dutta, V., et al., 2014.. Reduced ultraviolet light induced degradation and enhanced light harvesting using YVO₄:Eu³⁺ down-shifting nano-phosphor layer in organometal halide perovskite solar cells. *105. Appl. Phys. Lett.* <https://doi.org/10.1063/1.4891181>.
- Chang, C.Y., Chu, C.Y., Huang, Y.C., Huang, C.W., Chang, S.Y., Chen, C.A., et al., 2015. Tuning perovskite morphology by polymer additive for high efficiency solar cell. *ACS Appl. Mater. Interfaces* 7, 4955–4961. <https://doi.org/10.1021/acsm.5b00052>.
- Chapin, D.M., Fuller, C.S., Pearson, G.L., 1954. A new silicon p-n junction photocell for converting solar radiation into electrical power [3]. *J. Appl. Phys.* <https://doi.org/10.1063/1.1721711>.
- Chen, Q., Zhou, H., Hong, Z., Luo, S., Duan, H., Wang, H., et al., 2014. Planar heterojunction perovskite solar cells via vapor-assisted solution process, pp. 3–6. doi:10.1021/ja411509g.
- Chen, Min, Ju, Ming-Gang, Garces, Hector F., Carl, Alexander D., Ono, Luis K., Hawash, Zafer, Zhang, Yi, Shen, Tianyi, Qi, Yabing, Grimm, Ronald L., Pacifici, Domenico, Zeng, Xiao Cheng, Zhou, Yuan Yuan, Padture, Nitin P., 2019. Highly stable and efficient all-inorganic lead-free perovskite solar cells with native-oxide passivation. *Nat. Commun.* 10 (1). <https://doi.org/10.1038/s41467-018-07951-y>.
- Chen, J., Kim, S.G., Ren, X., Jung, H.S., Park, N.G., 2019. Effect of bidentate and tridentate additives on the photovoltaic performance and stability of perovskite solar cells. *J. Mater. Chem. A* 7, 4977–4987. <https://doi.org/10.1039/c8ta11977e>.
- Chen, W., Xu, L., Feng, X., Jie, J., He, Z., 2017. Metal acetylacetone series in interface engineering for full low-temperature-processed, high-performance, and stable planar perovskite solar cells with conversion efficiency over 16% on 1 cm² scale. *Adv. Mater.* 29, 1603923. <https://doi.org/10.1002/adma.201603923>.
- Cherrette, V.L., Hutcherson, C.J., Barnett, J.L., So, M.C., 2018. Fabrication and characterization of perovskite solar cells: an integrated laboratory experience. *J. Chem. Educ.* 95, 631–635. <https://doi.org/10.1021/acs.jchemed.7b00299>.
- Chess, C.A., Guloy, A.M., Feild, C.A., Mitzi, D.B., Wang, S., 2006. Conducting layered organic-inorganic halides containing <110>-oriented perovskite sheets. *Science* (80-) 267, 1473–1476. <https://doi.org/10.1126/science.267.5203.1473>.
- Chiang, C.-H., Lin, J.-W., Wu, C.-G., 2016. One-step fabrication of a mixed-halide perovskite film for a high-efficiency inverted solar cell and module. *J. Mater. Chem. A* 4, 13525–13533. <https://doi.org/10.1039/C6TA05209F>.
- Christians, J.A., Miranda Herrera, P.A., Kamat, P.V., 2015. Transformation of the excited state and photovoltaic efficiency of CH₃NH₃PbI₃ perovskite upon controlled exposure to humidified air. *J. Am. Chem. Soc.* 137, 1530–1538. <https://doi.org/10.1021/ja511132a>.
- Chung, I., Lee, B., He, J., Chang, R.P.H., Kanatzidis, M.G., 2012. All-solid-state dye-sensitized solar cells with high efficiency. *Nature* 485, 486–489. <https://doi.org/10.1038/nature11067>.
- Conings, B., Drijkoningen, J., Gauquelain, N., Babayigit, A., D'Haen, J., D'Olieslaeger, L., et al., 2015. Intrinsic thermal instability of methylammonium lead trihalide perovskite. *Adv. Energy Mater.* 5, 1–8. <https://doi.org/10.1002/aenm.201500477>.
- Conings, B., Drijkoningen, J., Gauquelain, N., Babayigit, A., Haen, J.D., Olieslaeger, L.D., et al., 2020. Intrinsic thermal instability of methylammonium lead trihalide perovskite, pp. 1–8. doi:10.1002/aenm.201500477.
- Continuing Progress in Perovskite Industrialization, Brings New Products to Customers, 2017. <https://www.solaronix.com/news/continuing-progress-in-perovskite-industrialization-brings-new-products-to-customers/> (accessed December 18, 2018).
- Daniel, B., Justin, S., Trystan, W., 2019. Perovskite solar cells in N-I-P structure with four slot-die-coated layers. *172158. R. Soc. Open Sci.* 5. <https://doi.org/10.1098/rsos.172158>.
- Das, J., Rene, E.R., Krishnan, J., Das, J., Er, R., Photocatalytic, K.J., 2018. Photocatalytic degradation of volatile pollutants. *J. Environ. Chem. Toxicol.* 2, 57–59.
- Deng, Y., Wang, Q., Yuan, Y., Huang, J., 2015. Vividly colorful hybrid perovskite solar cells by doctor-blade coating with perovskite photonic nanostructures. *Mater. Horizons* 2, 578–583. <https://doi.org/10.1039/C5MH00126A>.
- Deng, Y., Peng, E., Shao, Y., Xiao, Z., Dong, Q., Huang, J., 2015. Environmental science trihalide perovskite solar cells with doctor-bladed. *Energy Environ. Sci.* <https://doi.org/10.1039/C4EE03907F>.
- Di Giacomo, F., Shanmugam, S., Fledderus, H., Bruijnaers, B.J., Verhees, W.J.H., Dorenkamp, M.S., et al., 2018. Up-scalable sheet-to-sheet production of high efficiency perovskite module and solar cells on 6-in. substrate using slot die coating. *Sol. Energy Mater. Sol. Cells* 181, 53–59. <https://doi.org/10.1016/j.solmat.2017.11.010>.
- Divitini, G., Cacovich, S., Matteocci, F., Cinà, L., Di Carlo, A., Ducati, C., 2016. In situ observation of heat-induced degradation of perovskite solar cells. *Nat. Energy* 1, 15012. <https://doi.org/10.1038/NEENERGY.2015.12>.
- Docampo, P., Ball, J.M., Darwich, M., Eperon, G.E., Snaith, H.J., 2013. Efficient organometal trihalide perovskite planar-heterojunction solar cells on flexible polymer substrates. *Nat. Commun.* 4, 1–6. <https://doi.org/10.1038/ncomms3761>.
- Dyesol secures \$1 million grant for perovskite PV research, 2016. <https://www.perovskite-info.com/dyesol-secures-1-million-grant-perovskite-pv-research> (accessed November 10, 2018).
- Dyesol secures \$1 million grant for perovskite PV research. <https://www.perovskite-info.com/solliance-sets-145-cell-performance-record-large-perovskite-pv-modules> (accessed November 13, 2018).
- Eames, C., Frost, J.M., Barnes, P.R.F., O'Regan, B.C., Walsh, A., Islam, M.S., 2015. Ionic transport in hybrid lead iodide perovskite solar cells. *Nat. Commun.* 6, 2–9. <https://doi.org/10.1038/ncomms8497>.
- Eperon, G.E., Burlakov, V.M., Docampo, P., Goriely, A., Snaith, H.J., 2013. Morphological control for high performance, solution- processed planar heterojunction perovskite. *Sol. Cells* 1–7. <https://doi.org/10.1002/adfm.201302090>.
- Eperon, G.E., Stranks, S.D., Menelaou, C., Johnston, M.B., Herz, L.M., Snaith, H.J., 2014. Formamidinium lead trihalide: A broadly tunable perovskite for efficient planar heterojunction solar cells. *Energy Environ. Sci.* 7, 982–988. <https://doi.org/10.1039/c3ee43822h>.

- Eperon, G.E., Eperon, G.E., Leijtens, T., Bush, K.A., Prasanna, R., Green, T., et al., 2016. Eperon 2016 (9717), 1–10. <https://doi.org/10.1126/science.aaf9717>.
- Funding Opportunity Announcement: Solar Energy Technologies Office Fiscal Year 2019 Funding Program 2019. <https://www.energy.gov/eere/solar/funding-opportunity-announcement-solar-energy-technologies-office-fiscal-year-2019> (accessed June 5, 2019).
- Gardner, K.L., Tait, J.G., Merckx, T., Qiu, W., Paetzold, U.W., Kootstra, L., et al., 2016. Nonhazardous solvent systems for processing perovskite photovoltaics. *Adv. Energy Mater.* 6, 1–8. <https://doi.org/10.1002/aenm.201600386>.
- Giordano, F., Abate, A., Pablo, J., Baena, C., Saliba, M., Matsui, T., et al., 2016. Enhanced electronic properties in mesoporous TiO₂ via lithium doping for high-efficiency perovskite solar cells. *Nat. Commun.* 7, 1–6. <https://doi.org/10.1038/ncomms10379>.
- Grancini, G., Roldán-Carmona, C., Zimmermann, I., Mosconi, E., Lee, X., Martineau, D., et al., 2017. One-year stable perovskite solar cells by 2D/3D interface engineering. *Nat. Commun.* 8, 1–8. <https://doi.org/10.1038/ncomms15684>.
- GreatCell unveils its perovskite-based solar cells commercialization roadmap, 2018. <https://www.perovskite-info.com/greatcell-unveils-its-perovskite-based-solar-cells-commercialization-roadmap> (accessed February 7, 2019).
- Green, Martin A., Hishikawa, Yoshihiro, Dunlop, Ewan D., Levi, Dean H., Hohl-Ebinger, Jochen, Ho-Baillie, Anita W.Y., 2018. Solar cell efficiency tables (version 51). *Prog. Photovolt. Res. Appl.* 26 (1), 3–12. <https://doi.org/10.1002/pip.2978>.
- Habibi, M., Rahimzadeh, A., Bennoune, I., Eslamian, M., 2017. Defect-free large-area (25 cm²) light absorbing perovskite thin films made by spray coating. *Coatings* 7, 42. <https://doi.org/10.3390/coatings7030042>.
- Habisreutinger, S.N., Leijtens, T., Eperon, G.E., Stranks, S.D., Nicholas, R.J., Snaith, H.J., 2014. Carbon nanotube/polymer composites as a highly stable hole collection layer in perovskite solar cells. *Nano Lett.* 14, 5561–5568. <https://doi.org/10.1021/nl501982b>.
- Hagfeldt, A., Saliba, M., 2018. Perovskite solar cells on a planar architecture, 3583, pp. 1–9.
- Haider, M., Zhen, C., Wu, T., Liu, G., Cheng, H., 2018. Journal of Materials Science & Technology Boosting efficiency and stability of perovskite solar cells with nickel phthalocyanine as a low-cost hole transporting layer material. *J. Mater. Sci. Technol.* 34, 1474–1480. <https://doi.org/10.1016/j.jmst.2018.03.005>.
- Hao, F., Stoumpos, C.C., Chang, R.P.H., Kanatzidis, M.G., 2014. Supporting information for anomalous band gap behavior in mixed Sn and Pb perovskites enables broadening of absorption spectrum in solar cells anomalous band gap behavior in mixed Sn and Pb perovskites enables broadening of absorption spectrum in solar ce. *J. Am. Chem. Soc.* 136, 8094–8099. <https://doi.org/10.1021/ja5033259>.
- Hao, F., Stoumpos, K., Cao, D.H., Chang, R.P.H., Kanatzidis, M., 2014. Lead-free solid-state organic-inorganic halide perovskite solar cells. *Nat. Photonics* 8 (6), 489–494. <https://doi.org/10.1038/nphoton.2014.82> n.d.
- Haruyama, J., Sodeyama, K., Han, L., Tateyama, Y., 2015. First-principles study of ion diffusion in perovskite solar cell sensitizers. *J. Am. Chem. Soc.* 137, 10048–10051. <https://doi.org/10.1021/jacs.5b03615>.
- Hendriks, K.H., Van Franeker, J.J., Bruijnaers, B.J., Anta, J.A., Wienk, M.M., Janssen, R.A.J., 2017. 2-Methoxyethanol as a new solvent for processing methylammonium lead halide perovskite solar cells. *J. Mater. Chem. A* 5, 2346–2354. <https://doi.org/10.1039/C6TA09125C>.
- Heo, J.H., Im, S.H., Noh, J.H., Mandal, T.N., Lim, C., Chang, J.A., et al. Solar cells containing perovskite compound and 2013:1–6. doi:10.1038/NPHOTON.2013.80.
- Highly efficient solar cells thanks to solid foundation, 2019. http://www.kit.edu/kit/pi_2019_097_hocheffiziente-solarzellen-dank-solidem-fundament.php (accessed July 6, 2019).
- Hirayama, M., Ishihara, T., Goto, T., Uchida, K., Miura, N., 1994. Magnetoabsorption of the lowest exciton in perovskite-type compound (CH₃NH₃)PbI₃. *Phys. B Phys. Condens. Matter.* 201, 427–430. [https://doi.org/10.1016/0921-4526\(94\)91130-4](https://doi.org/10.1016/0921-4526(94)91130-4).
- Holzhey, P., Saliba, M., 2018. A full overview of international standards assessing the long-term stability of perovskite solar cells. *J. Mater. Chem. A* 6, 21794–21808. <https://doi.org/10.1039/C8TA06950F>.
- Hsieh, H., Yu, J., Rwei, S., Lin, K., Shih, Y., 2018. Ultra-compact titanium oxide prepared by ultrasonic spray pyrolysis method for planar heterojunction perovskite hybrid solar cells. *Thin Solid Films* 659, 41–47. <https://doi.org/10.1016/j.tsf.2018.05.002>.
- Hu, Y., Aygüler, M.F., Petrus, M.L., Bein, T., Docampo, P., 2017. Impact of rubidium and cesium cations on the moisture stability of multiple-cation mixed-halide perovskites. *ACS Energy Lett.* 2, 2212–2218. <https://doi.org/10.1021/acsenergylett.7b00731>.
- Huang, F., Li, M., Siffalovic, P., 2018. Environmental science from scalable solution fabrication of perovskite films towards commercialization of solar cells, doi:10.1039/c8ee03025a.
- Huang, J., Xiang, S., Yu, J., Li, C.Z., 2019. Highly efficient prismatic perovskite solar cells. *Energy Environ. Sci.* 12, 929–937. <https://doi.org/10.1039/c8ee02575d>.
- Hwang, I., Jeong, I., Lee, J., Ko, M.J., Yong, K., 2015. Enhancing stability of perovskite solar cells to moisture by the facile hydrophobic passivation. *ACS Appl. Mater. Interfaces* 7, 17330–17336. <https://doi.org/10.1021/acsami.5b04490>.
- Im, J., Jang, I., Pellet, N., Park, N., 2014. Size for high-efficiency perovskite solar cells, 1–6. doi:10.1038/nano.2014.181.
- Im, Jeong-Hyeok, Lee, Chang-Ryul, Lee, Jin-Wook, Park, Sang-Won, Park, Nam-Gyu, 2011. 6.5% efficient perovskite quantum-dot-sensitized solar cell. *Nanoscale* 3 (10), 4088. <https://doi.org/10.1039/c1nr10867k>.
- IMEC AND SOLLIANCE'S PEROVSKITE PV MODULES ACHIEVE 12.4% 2017. <https://www.solliance.eu/2017/perovskite-modules-achieve-12-4pt> (accessed May 25, 2018).
- Information, S., 2013. General working principles of CH 3 NH 3 PbX₃ perovskite solar cells, 2–5, doi:10.1021/nl404252e.
- Interview with Greatcell Solar Materials' GM Yanek Hebing, 2019. <https://www.perovskite-info.com/interview-greatcell-solar-materials-gm-yanek-hebing> (accessed June 2, 2019).
- Ito, S., Tanaka, S., Manabe, K., Nishino, H., 2014. Effects of surface blocking layer of Sb₂S₃ on nanocrystalline TiO₂ for CH₃NH₃PbI₃ perovskite solar cells. *J. Phys. Chem. C* 118, 16995–17000. <https://doi.org/10.1021/jp500449z>.
- Jeon, N.J., Noh, J.H., Kim, Y.C., Yang, W.S., Ryu, S., Il, Seok S., 2014. Solvent engineering for high-performance inorganic-organic hybrid perovskite solar cells. *Nat. Mater.* 13, 897–903. <https://doi.org/10.1038/nmat4014>.
- Jeon, N.J., Noh, J.H., Yang, W.S., Kim, Y.C., Ryu, S., Seo, J., et al., 2015. Compositional engineering of perovskite materials for high-performance solar cells. *Nature* 517, 476–480. <https://doi.org/10.1038/nature14133>.
- Jiang, M., Niu, Q., Tang, X., Zhang, H., Xu, H., Huang, W., Yao, J., Yan, B., Xia, R., 2019. Improving the performances of perovskite solar cells via modification of electron transport layer. *Polymers (Basel)*, 11. <https://doi.org/10.3390/polym11010147>.
- Jiang, Y., Qiu, L., Juarez-Perez, E.J., Ono, L.K., Hu, Z., Liu, Z., et al., 2019. Reduction of lead leakage from damaged lead halide perovskite solar modules using self-healing polymer-based encapsulation. *Nat. Energy* 4. <https://doi.org/10.1038/s41560-019-0406-2>.
- Jin, J., Li, H., Chen, C., Zhang, B., Xu, L., Dong, B., et al., 2017. Enhanced performance of perovskite solar cells with zinc chloride additives. *ACS Appl. Mater. Interfaces* 9, 42875–42882. <https://doi.org/10.1021/acsami.7b15310>.
- Adv. Mater. 31 (2), 1804835. <https://doi.org/10.1002/adma.v31.210.1002/adma.201804835>.
- Joon Jung, H., Kim, D., Kim, S., Shin, B., Dravid, V.P., 2017. Operando injection of oxygen ions to organometal halide perovskite (CH 3 NH 3 P 3) under in-situ electrical biasing STEM-EELS. *Microsc. Microanal.* 23, 1976–1977. <https://doi.org/10.1017/s14319276171010546>.
- Jung, E.H., Jeon, N.J., Park, E.Y., Moon, C.S., Shin, T.J., Yang, T.Y., et al., 2019. Efficient, stable and scalable perovskite solar cells using poly(3-hexylthiophene). *Nature* 567, 511–515. <https://doi.org/10.1038/s41586-019-1036-3>.
- Kavadiya, S., Niedzwiedzki, D.M., Huang, S., Biswas, P., 2017. Electrospray-assisted fabrication of moisture-resistant and highly stable perovskite solar cells at ambient conditions. *Adv. Energy Mater.* 7, 1–9. <https://doi.org/10.1002/aenm.201700210>.
- Kim, H., Seo, J., Park, N., 2016. Material and device stability in perovskite solar cells, pp. 2528–2540. doi:10.1002/cscs.201600915.
- Kim, H., Hagfeldt, A., Park, N., 2019. Morphological and compositional progress in halide perovskite solar cells, pp. 1192–200. doi:10.1039/c8cc08653b.
- Kim, H.S., Im, S.H., Park, N.G., 2014. Organolead halide perovskite: New horizons in solar cell research. *J. Phys. Chem. C*. <https://doi.org/10.1021/jp409025w>.
- Kim, H., Lee, C., Im, J., Lee, K., Moehl, T., Marchioro, A., et al., 2012. All-Solid-State Submicron Thin Film 1–7. <https://doi.org/10.1038/srep00591>.
- Kojima, A., Teshima, K., Shirai, Y., Miyasaka, T., 2009. Organometal Halide Perovskites as Visible-Light Sensitizers for Photovoltaic 6050–6051. <https://doi.org/10.1021/ja809598r>.
- Kosasih, F.U., Ducati, C., 2018. Characterising degradation of perovskite solar cells through in-situ and operando electron microscopy. *Nano Energy* 47, 243–256. <https://doi.org/10.1016/j.nanoen.2018.02.055>.
- Köster, U., 1978. Crystallization of amorphous silicon films. *Phys. Status Solidi* 48, 313–321. <https://doi.org/10.1002/pssa.2210480207>.
- Kumar, M.H., Dharani, S., Leong, W.L., Boix, P.P., Prabhakar, R.R., Baikie, T., Shi, C., Ding, H., Ramesh, R., Asta, M., Graetzel, M., Mhaisalkar, S.G., Mathews, N., 2014. Lead-free halide perovskite solar cells with high photocurrents realized through vacancy modulation. *Adv. Mater.* 26, 7122–7127. <https://doi.org/10.1002/adma.201401991>.
- Kwon, Y.S., Lim, J., Yun, H.J., Kim, Y.H., Park, T., 2014. A diketopyrrolopyrrole-containing hole transporting conjugated polymer for use in efficient stable organic-inorganic hybrid solar cells based on a perovskite. *Energy Environ. Sci.* 1454–1460.
- Lee, S., Kang, D., 2017. Highly efficient and stable sn-rich perovskite solar cells by introducing bromine highly efficient and stable Sn-rich perovskite solar cells by introducing bromine, doi:10.1021/acsami.7b04011.
- J. Am. Chem. Soc. 136 (43), 15379–15385. <https://doi.org/10.1021/ja508464w>.
- Leijtens, T., Eperon, G.E., Pathak, S., Abate, A., Lee, M.M., Snaith, H.J., 2013. Overcoming ultraviolet light instability of sensitized TiO₂ with meso-superstructured organometal tri-halide perovskite solar cells. *Nat. Commun.* 4, 1–8. <https://doi.org/10.1038/ncomms3885>.
- Leijtens, T., Hoke, E.T., Grancini, G., Slotcavage, D.J., Eperon, G.E., Ball, J.M., et al., 2015. Mapping electric field-induced switchable poling and structural degradation in hybrid lead halide perovskite thin films. *Adv. Energy Mater.* 5, 1–11. <https://doi.org/10.1002/aenm.201500962>.
- Leo, K., 2015. Signs of stability. *Nat. Nanotechnol.* 10, 574–575. <https://doi.org/10.1038/nano.2015.139>.
- Li, Xiong, Bi, Dongqin, Yi, Chenyi, Décopet, Jean-David, Luo, Jingshan, Zakeeruddin, Shaik Mohammed, Hagfeldt, Anders, Grätzel, Michael, 2016. A vacuum flash-assisted solution process for high-efficiency large-area perovskite solar cells. *Science* 353 (6294), 58–62. <https://doi.org/10.1126/scienceaa8060>.
- Li, C., Lu, X., Ding, W., Feng, L., Gao, Y., Guo, Z., 2008. Formability of ABX₃ (X = F, Cl, Br, I) halide perovskites. *Acta Crystallogr. B* 64, 702–707. <https://doi.org/10.1107/S0108768108032734>.
- Li, T., Pan, Y., Wang, Z., Xia, Y., Chen, Y., Huang, W., 2017. Additive engineering for highly efficient organic-inorganic halide perovskite solar cells: Recent advances and perspectives. *J. Mater. Chem. A* 5, 12602–12652. <https://doi.org/10.1039/c7ta07198g>.
- Li, C., Soh, K.C.K., Wu, P., 2004. Formability of ABO₃ perovskites. *J. Alloy. Compd.* 372, 40–48. <https://doi.org/10.1016/j.jallcom.2003.10.017>.
- Li, Z., Xiao, C., Yang, Y., Harvey, S.P., Kim, D.H., Christians, J.A., Yang, M., Schulz, P., Nanayakkara, S.U., Jiang, C.-S., Luther, J.M., Berry, J.J., Beard, M.C., Al-Jassim KZ., M.M., 2017. Extrinsic ion migration in perovskite solar cells. *Energy Environ. Sci.*

- <https://doi.org/10.1039/C7EE00358G>.
- Liang, K., Mitzi, D.B., Prikas, M.T., 2013. cSynthesis and Characterization off.pdf 4756, 403–411.
- Liang, Yangang, Yao, Yangyi, Zhang, Xiaohang, Hsu, Wei-Lun, Gong, Yunhui, Shin, Jongmoon, Wachsman, Eric D., Dagenais, Mario, Takeuchi, Ichiro, 2016. Fabrication of organic-inorganic perovskite thin films for planar solar cells via pulsed laser deposition. AIP Adv. 6 (1), 015001. <https://doi.org/10.1063/1.4939621>.
- Liao, W., Zhao, D., Yu, Y., Shrestha, N., Ghimire, K., Grice, C.R., et al., 2016. Fabrication of efficient low-bandgap perovskite solar cells by combining formamidinium tin iodide with methylammonium lead Iodide, doi:10.1021/jacs.6b08337.
- Liu, C., Ding, W., Zhou, X., Gao, J., Cheng, C., Zhao, X., et al., 2017. Efficient and stable perovskite solar cells prepared in ambient air based on surface-modified perovskite layer. J. Phys. Chem. C 121, 6546–6553. <https://doi.org/10.1021/acs.jpcc.7b00847>.
- Liu, M., Johnston, M.B., Snaith, H.J., 2013. Efficient planar heterojunction perovskite solar cells by vapour deposition. Nature 501, 395–398. <https://doi.org/10.1038/nature12509>.
- Liu, X., Liu, Z., Sun, B., Tan, X., Ye, H., Tu, Y., et al., 2018. 17.46% efficient and highly stable carbon-based planar perovskite solar cells employing Ni-doped rutile TiO₂ as electron transport layer. Nano Energy 50, 201–211. <https://doi.org/10.1016/j.nanoen.2018.05.031>.
- Lyu, M., Yun, J.H., Chen, P., Hao, M., Wang, L., 2017.. Addressing toxicity of lead: progress and applications of low-toxic metal halide perovskites and their derivatives. Adv. Energy Mater. 7. <https://doi.org/10.1002/aenm.201602512>.
- Mahmood, K., Taqi, M., 2017. RSC Advances Current status of electron transport layers in perovskite solar cells : materials and properties. RSC Adv. 7, 17044–17062. <https://doi.org/10.1039/C7RA00002B>.
- Mahmood, K., Swain, B.S., Jung, H.S., 2014. Controlling the surface nanostructure of ZnO and Al-doped ZnO thin films using electrostatic spraying for their application in 12% efficient perovskite solar cells. Nanoscale 6, 9127–9138. <https://doi.org/10.1039/c4nr02065k>.
- Matthes, F., Eggers, H., Richards, B.S., Hernandez-sosa, G., Lemmer, U., Paetzold, U.W., 2018. Inkjet-printed triple cation perovskite solar cells. ACS Appl. Energy Mater. 1, 1834–1839. <https://doi.org/10.1021/acsaem.8b00222>.
- Matteocci, F., Razza, S., Di Giacomo, F., Casaluci, S., Minuzzi, G., Brown, T.M., et al., 2014. Solid-state solar modules based on mesoscopic organometallic halide perovskite: A route towards the up-scaling process. Phys. Chem. Chem. Phys. 16, 3918–3923. <https://doi.org/10.1039/c3cp55313b>.
- Mehmood, U., Al-ahmed, A., Afzaal, M., Al-sulaiman, F.A., 2017. Recent progress and remaining challenges in organometallic halides based perovskite solar cells. Renew. Sustain. Energy Rev. 78, 1–14. <https://doi.org/10.1016/j.rser.2017.04.105>.
- Mei, A., Li, X., Liu, L., Ku, Z., Liu, T., Rong, Y., Xu, M., Hu, M., Chen, J., Yang, Y., Gratzel, M., Han, H., 2014. A hole-conductor-free, fully printable mesoscopic perovskite solar cell with high stability. Science 345 (6194), 295–298. <https://doi.org/10.1126/science.1254763>.
- Microquanta achieves 14.24% efficiency with large-area perovskite solar module, 2019. <https://www.pv-magazine.com/2019/10/24/microquanta-achieves-14-24-efficiency-with-large-area-perovskite-solar-module/> (accessed November 30, 2019).
- Minemoto, Takashi, Murata, Masashi, 2014. Device modeling of perovskite solar cells based on structural similarity with thin film inorganic semiconductor solar cells. J. Appl. Phys. 116 (5), 054505. <https://doi.org/10.1063/1.4891982>.
- Mitzi, D.B., Chondroudis, K., Kagan, C.R., 1999. Design structure, and optical properties of organic – inorganic perovskites containing an oligothiophene chromophore. Inorg. Chem. 38, 6246–6256. <https://doi.org/10.1021/ic991048k>.
- Mitzi, D.B., Chondroudis, K., Kagan, C.R., 2010. Organic-inorganic electronics. IBM J. Res. Dev. 45, 29–45. <https://doi.org/10.1147/rd.451.0029>.
- Miyata, A., Mitioglu, A., Plochocka, P., Portugal, O., Wang, J.T.W., Stranks, S.D., et al., 2015. Direct measurement of the exciton binding energy and effective masses for charge carriers in organic-inorganic tri-halide perovskites. Nat. Phys. 11, 582–587. <https://doi.org/10.1038/nphys3357>.
- Moore, D.T., Sai, H., Tan, K.W., Smilgies, D.M., Zhang, W., Snaith, H.J., et al., 2015. Crystallization kinetics of organic-inorganic trihalide perovskites and the role of the lead anion in crystal growth. J. Am. Chem. Soc. 137, 2350–2358. <https://doi.org/10.1021/ja512117e>.
- Nazeeruddin, M.K., Han, H., Grätzel, M., 2015. Alkylphosphonic acid ω -ammonium chlorides. Nat. Chem. 1–9. <https://doi.org/10.1038/nchem.2324>.
- Nie, W., Tsai, H., Asadpour, R., Neukirch, A.J., Gupta, G., Crochet, J.J., Chhowalla, M., Tretiak, S., Alam, M.A., Wang, H., 2015. High-efficiency solution-processed perovskite solar cells with millimeter-scale grains. Science (80 -) 347, 522–526.
- Niu, G., Guo, X., Wang, L., 2015. Review of recent progress in chemical stability of perovskite solar cells. J. Mater. Chem. A. <https://doi.org/10.1039/c4ta04994b>.
- Niu, G., Guo, X., Wang, L., 2015. Review of recent progress in chemical stability of perovskite solar cells. J. Mater. Chem. A 3, 8970–8980. <https://doi.org/10.1039/c4ta04994b>.
- Noel, N.K., Stranks, S.D., Abate, A., Wehrenfennig, C., Guarnera, S., Haghhighirad, A., et al., 2014. Environmental Science for photovoltaic applications †. Energy Environ. Sci. 7, 3061–3068. <https://doi.org/10.1039/C4EE01076K>.
- Noel, N.K., Habersreutinger, S.N., Wenger, B., Klug, M.T., Hörrnther, M.T., Johnston, M.B., et al., 2017. A low viscosity, low boiling point, clean solvent system for the rapid crystallisation of highly specular perovskite films. Energy Environ. Sci. 10, 145–152. <https://doi.org/10.1039/c6ee02373h>.
- Noh, J.H., Im, S.H., Heo, J.H., Mandal, T.N., Seok, S. Il., 2013. Nano Lett. 13, 1764–1769. <https://doi.org/10.1021/nl400349b>.
- NREL Efficiency Chart, 2019. www.nrel.gov/pv/assets/pdfs/best-research-cell-efficiencies-190416.pdf.
- NREL PV Research Cell Record Efficiency Chart 2019.
- Ogomi, Y., Morita, A., Tsukamoto, S., Saitho, T., Fujikawa, N., Shen, Q., et al., 2014. CH₃NH₃Sn_xPb_x-I₃ perovskite solar cells covering up to 1060 nm. J. Phys. Chem. Lett. 5, 1004–1011.
- Omondi, C.A., 2018. Investigation of hybrid organic-inorganic lead halide perovskites by modulated surface photovoltage spectroscopy Vorgelegt von. Dissertation. <https://doi.org/10.14279/depositone-7257>.
- Oxford PV perovskite solar cell achieves 28% efficiency 2018. <https://www.oxfordpv.com/news/oxford-pv-perovskite-solar-cell-achieves-28-efficiency> (accessed May 20, 2019).
- Oxford PV to collaborate with Meyer Burger, 2019. <https://www.oxfordpv.com/news/oxford-pv-collaborate-meyer-burger> (accessed June 16, 2019).
- PANASONIC JOINS SOLLIANCE AS AN INDUSTRIAL PARTNER, 2019. <https://www.solliance.eu/2016/panasonic-joins-solliance-as-an-industrial-partner> (accessed July 14, 2019).
- Park, B.W., Philippe, B., Zhang, X., Rensmo, H., Boschloo, G., Johansson, E.M.J., 2015. Bismuth based hybrid perovskites a3bi2I9 (a: methylammonium or cesium) for solar cell application. Mater. Adv. <https://doi.org/10.1002/adma.201501978>.
- Park, N., 2015. Highly reproducible perovskite solar cells with average efficiency of 18.3% and best efficiency of 19.7% fabricated via lewis base adduct of lead(II) Iodide, pp. 16–9, doi:10.1021/jacs.5b04930.
- Peng, X., Yuan, J., Shen, S., Gao, M., Chesman, A.S.R., Yin, H., et al., 2017.. Perovskite and organic solar cells fabricated by inkjet printing: progress and prospects. Adv. Funct. Mater. 27. <https://doi.org/10.1002/adfm.201703704>.
- Perovskite companies: the comprehensive list, 2018. <https://www.perovskite-info.com/companies> (accessed November 21, 2018).
- Philippe, B., Park, B.W., Lindblad, R., Oscarsson, J., Ahmadi, S., Johansson, E.M.J., Rensmo, H., 2015. Chemical and electronic structure characterization of lead halide perovskites and stability behavior under different exposures-A photoelectron spectroscopy investigation. Chem. Mater. 27, 1720–1731. <https://doi.org/10.1021/acs.chemmater.5b00348>.
- Pisoni, A., Jacićović, J., Barišić, O.S., Spina, M., Gaál, R., Forró, L., et al., 2014. Ultra-low thermal conductivity in organic-inorganic hybrid perovskite CH₃NH₃PbI₃. J. Phys. Chem. Lett. 5, 2488–2492. <https://doi.org/10.1021/jz5012109>.
- Pitchaiya, S., Natarajan, M., 2020. REVIEW ARTICLE A review on the classification of organic / inorganic / carbonaceous hole transporting materials for perovskite solar cell application. Arab. J. Chem. 13, 2526–2557. <https://doi.org/10.1016/j.arabjc.2018.06.006>.
- Qian, J., Ernst, M., Wu, N., Blakers, A., 2019. Impact of perovskite solar cell degradation on the lifetime energy yield and economic viability of perovskite/silicon tandem modules. Sustain. Energy Fuels 3, 1439–1447. <https://doi.org/10.1039/c9se00143c>.
- Qiu, L., Liu, Z., Ono, L.K., Jiang, Y., Son, D.Y., Hawash, Z., et al., 2018. Scalable fabrication of stable high efficiency perovskite solar cells and modules utilizing room temperature sputtered SnO₂ electron transport layer. Adv. Funct. Mater. 1806779, 1–9. <https://doi.org/10.1002/adfm.201806779>.
- Ramirez, I., Zhang, J., Ducati, C., Grovenor, C., Johnston, M.B., Ginger, D.S., et al., 2016. Environmental science. Energy Environ. Sci. 9, 2892–2901. <https://doi.org/10.1039/C6EE01969B>.
- Ran, C., Xu, J., Gao, W., Huang, C., Dou, S., 2018. Chem. Soc. Rev. 4581–4610. <https://doi.org/10.1039/c7cs00868f>.
- Razza, S., Di Giacomo, F., Matteocci, F., Cinà, L., Palma, A.L., Casaluci, S., et al., 2015. Perovskite solar cells and large area modules (100 cm²) based on an air flow-assisted PbI₂ blade coating deposition process. J. Power Sources 277, 286–291. <https://doi.org/10.1016/j.jpowsour.2014.12.008>.
- Richardson, G., Foster, J.M., Walker, A.B., 2019. Environmental science how transport layer properties affect perovskite solar cell performance : insights from a coupled charge transport / ion migration model †, pp. 396–409, doi:10.1039/c8ee01576g.
- Roose, B., Johansen, C.M., Dupraz, K., Jaouen, T., Aebi, P., Steiner, U., et al., 2018. A Ga-doped SnO₂ mesoporous contact for UV stable highly efficient perovskite solar cells. J. Mater. Chem. A 6, 1850–1857. <https://doi.org/10.1039/c7ta07663k>.
- Saliba, M., Correa-Baena, J.P., Wolff, C.M., Stolterfoht, M., Phung, N., Albrecht, S., Neher, D., Abate, A., 2018. How to Make over 20% Efficient Perovskite Solar Cells in Regular (n-i-p) and Inverted (p-i-n) Architectures. Chem. Mater. 30, 4193–4201. <https://doi.org/10.1021/acs.chemmater.8b00136>.
- Sanchez, R.S., Gonzalez-Pedro, V., Lee, J.W., Park, N.G., Kang, Y.S., Mora-Sero, I., et al., 2014. Slow dynamic processes in lead halide perovskite solar cells. Characteristic times and hysteresis. J. Phys. Chem. Lett. 5, 2357–2363. <https://doi.org/10.1021/jz5011187>.
- Sarikka, T., Ulla, V., 2017. Solar cells with humidity assisted thermal treatment †, pp. 12060–7, doi:10.1039/C7TA04132B.
- Sarukura, N., Murakami, H., Estacio, E., Ono, S., El Ouenzerfi, R., Cadatal, M., et al., 2007. Proposed design principle of fluoride-based materials for deep ultraviolet light emitting devices. Opt. Mater. (Amst) 30, 15–17. <https://doi.org/10.1016/j.optmat.2006.11.031>.
- Saule Technologies on its way to launching prototype production line in Q4 2019, 2019. <https://www.perovskite-info.com/saule-technologies-its-way-launching-prototype-production-line-q4-2019> (accessed July 7, 2019).
- Saule Technologies' perovskite solar panel installed in innovative Japanese hotel, 2018. <https://www.perovskite-info.com/saule-technologies-perovskite-solar-panel-installed-innovative-japanese-hotel> (accessed May 15, 2019).
- Saule Technologies' perovskite-based solar panels headed for commercial implementation by building company Skanska, 2018. <https://www.perovskite-info.com/saule-technologies-perovskite-based-solar-panels-headed-commercial-implementation-building-company> (accessed December 19, 2018).
- Schultes, M., Giesbrecht, N., Kueffner, J., Docampo, P., Bein, T., Powalla, M., 2019. Universal nanoparticle wetting agent for upscaling perovskite. Sol. Cells. <https://doi.org/10.1021/acsami.8b22206>.
- Shaikh, J.S., Shaikh, N.S., Sheik, A.D., Kale, A.J., Kanjanaboos, P., Kook, C., et al., 2017.

- Perovskite solar cells : In pursuit of efficiency and stability. *Mater. Des.* 136, 54–80. <https://doi.org/10.1016/j.matdes.2017.09.037>.
- Shao, S., Liu, J., Portale, G., Fang, H.H., Blake, G.R., ten Brink, G.H., Koster, L.J.A., Loi, M.A., 2018. Highly Reproducible Sn-Based Hybrid Perovskite Solar Cells with 9% Efficiency. *Adv. Energy Mater.* 8. <https://doi.org/10.1002/aenm.201702019>.
- Shao, S., Liu, J., Portale, G., Fang, H.H., Blake, G.R., ten Brink, G.H., et al., 2018. Highly reproducible Sn-based hybrid perovskite solar cells with 9% efficiency. *Adv. Energy Mater.* 8. <https://doi.org/10.1002/aenm.201702019>.
- Shi, J., Dong, J., Lv, S., Xu, Y., Zhu, L., Xiao, J., et al., 2014. Hole-conductor-free perovskite organic lead iodide heterojunction thin-film solar cells: High efficiency and junction property. *Appl. Phys. Lett.*(104). <https://doi.org/10.1063/1.4864638>.
- Shin, H.O., Kim, B.M., Jang, T., Kim, K.M., Roh, D.H., Nam, J.S., Kim, J.S., Kim, U.Y., Lee, B., Pang, Y., Kwon, T.H., 2019. Surface State-Mediated Charge Transfer of Cs₂Ni₆ and Its Application in Dye-Sensitized Solar Cells. *Adv. Energy Mater.* 9, 1–8. <https://doi.org/10.1002/aenm.201803243>.
- Shirazi, M., Reza, M., Reza, T., Dariani, S., Taghi, M., 2018. Fabrication of hole-conductor-free perovskite solar cells based on Al doped ZnO and low-cost carbon electrode. *J. Mater. Sci.: Mater. Electron.* 29, 10092–10101. <https://doi.org/10.1007/s10854-018-9054-8>.
- Smith, I.C., Hoke, E.T., Solis-Ibarra, D., McGehee, M.D., Karunadasa, H.I., 2014. A layered hybrid perovskite solar-cell absorber with enhanced moisture stability. *Angew. Chem. – Int. Ed.* 53, 11232–11235. <https://doi.org/10.1002/anie.201406466>.
- Snaith, H.J., 2013. Perovskites: The emergence of a new era for low-cost, high-efficiency solar cells. *J. Phys. Chem. Lett.* 4, 3623–3630. <https://doi.org/10.1021/jz4020162>.
- Solaronix Achieves Major Breakthrough Toward Perovskite Solar Cell Industrialization, 2016. <https://www.solaronix.com/news/solaronix-achieves-major-breakthrough-toward-perovskite-solar-cell-industrialization> (accessed December 18, 2018).
- Steele, Julian A., Jin, Handong, Dovgaluk, Iurii, Berger, Robert F., Braeckeveldt, Tom, Yuan, Haifeng, Martin, Cristina, Solano, Eduardo, Lejaeghere, Kurt, Rogge, Sven M.J., Notebaert, Charlotte, Vandezande, Wouter, Janssen, Kris P.F., Goderis, Bart, Debroye, Elke, Wang, Ya-Kun, Dong, Yitong, Ma, Dongxin, Saidaminov, Makhsum, Tan, Hairen, Lu, Zhenghong, Dyadkin, Vadim, Chernyshov, Dmitry, Van Speybroeck, Veronique, Sargent, Edward H., Hofkens, Johan, Roeffaers, Maarten B.J., 2019. Thermal nonequilibrium of strained black CsPbI₃ thin films. *Science* 365 (6454), 679–684. <https://doi.org/10.1126/science:aax3878>.
- Stoumpos, C.C., Malliakas, C.D., Kanatzidis, M.G., 2013. Semiconducting tin and lead iodide perovskites with organic cations: Phase transitions, high mobilities, and near-infrared photoluminescent properties. *Inorg. Chem.* 52, 9019–9038. <https://doi.org/10.1021/ic401215x>.
- Sun, X., Zhang, C., Chang, J., Yang, H., Xi, H., Lu, G., et al., 2016. Mixed-solvent-vapor annealing of perovskite for photovoltaic device efficiency enhancement. *Nano Energy* 28, 417–425. <https://doi.org/10.1016/j.nanoen.2016.08.055>.
- Supasai, T., Rujisanpan, N., Ullrich, K., Chemseddine, A., Dittrich, T., 2013. Formation of a passivating CH₃NH₃PbI₃/PbI₂ interface during moderate heating of CH₃NH₃PbI₃ layers. *Appl. Phys. Lett.* 103, 1–4. <https://doi.org/10.1063/1.4826116>.
- Tai, Q., Guo, X., Tang, G., You, P., Ng, T.W., Shen, D., et al., 2019. Antioxidant grain passivation for air-stable tin-based perovskite solar cells. *Angew. Chem. – Int. Ed.* 58, 806–810. <https://doi.org/10.1002/anie.201811539>.
- Tang, J., Jiao, D., Zhang, L., Zhang, X., Xu, X., Yao, C., et al., 2018. High-performance inverted planar perovskite solar cells based on efficient hole-transporting layers from well-crystalline NiO nanocrystals. *Sol. Energy* 161, 100–108. <https://doi.org/10.1016/j.solener.2017.12.045>.
- Tax, F.E., Feldmann, K.A., Galbraith, D.W., Feyereisen, R., Johnson, E.F., Meharennia, Y.T., et al., 2012. References and Notes 15 (2), 1084–1087.
- The History of Solar Energy, 2013. <https://energyinformative.org/the-history-of-solar-energy-timeline/> (accessed May 24, 2019).
- The International Renewable Energy Agency (IRENA), 2012. Renewable Energy Technologies: Cost Analysis Series, 1, 17.
- Thind, A.S., Kavadiya, S., Kouhnavaud, M., Wheelus, R., Cho, S.B., Lin, L.Y., et al., 2019. KBaTeBiO₆: A lead-free, inorganic double-perovskite semiconductor for photovoltaic applications. *Chem. Mater.* 31, 4769–4778. <https://doi.org/10.1021/acs.chemmater.9b01025>.
- Toshiba Develops 703cm² Film-based Perovskite Photovoltaic Module With a 11.7 Percent Power Conversion Efficiency, 2018. <https://www cdrinfo.com/Sections/News/Print.aspx?NewsId=70171> (accessed December 21, 2018).
- Travis, W., Glover, E.N.K., Bronstein, H., Scanlon, D.O., Palgrave, R.G., 2016. On the application of the tolerance factor to inorganic and hybrid halide perovskites: A revised system. *Chem. Sci.* 7, 4548–4556. <https://doi.org/10.1039/c5sc04845a>.
- Tress, W., Marinova, N., Moehl, T., Zakeeruddin, S.M., Nazeeruddin, M.K., Grätzel, M., 2015. Understanding the rate-dependent J-V hysteresis, slow time component, and aging in CH₃NH₃PbI₃ perovskite solar cells: The role of a compensated electric field. *Energy Environ. Sci.* 8, 995–1004. <https://doi.org/10.1039/c4ee03664f>.
- Unger, E.L., Hoke, E.T., Bailie, C.D., Nguyen, W.H., Bowring, A.R., Heumüller, T., et al., 2014. Hysteresis and transient behavior in current-voltage measurements of hybrid-perovskite absorber solar cells. *Energy Environ. Sci.* 7, 3690–3698. <https://doi.org/10.1039/c4ee02465f>.
- Vak, D., Hwang, K., Faulks, A., Jung, Y.S., Clark, N., Kim, D.Y., et al., 2015. 3D printer based slot-die coater as a lab-to-fab translation tool for solution-processed solar cells. *Adv. Energy Mater.* 5, 1–8. <https://doi.org/10.1002/aenm.201401539>.
- Valverde-Chávez, D.A., Ponseca, C.S., Stoumpos, C.C., Yartsev, A., Kanatzidis, M.G., Sundström, V., et al., 2015. Intrinsic femtosecond charge generation dynamics in single crystal CH₃NH₃PbI₃. *Energy Environ. Sci.* 8, 3700–3707. <https://doi.org/10.1039/c5ee02503f>.
- Van Reenen, S., Kemerink, M., Snaith, H.J., 2015. Modeling anomalous hysteresis in perovskite solar cells. *J. Phys. Chem. Lett.* 6, 3808–3814. <https://doi.org/10.1021/acscjpcllett.5b01645>.
- Wang, Q., Chen, B., Liu, Y., Deng, Y., Bai, Y., Dong, Q., et al., 2017. Scaling behavior of moisture-induced grain degradation in polycrystalline hybrid perovskite thin films. *Energy Environ. Sci.* 10, 516–522. <https://doi.org/10.1039/C6EE02941H>.
- Wang, Z.K., Li, M., Yang, Y.G., Hu, Y., Ma, H., Gao, X.Y., Liao, L.S., 2016. High Efficiency Pb-In Binary Metal Perovskite Solar Cells. *Adv. Mater.* 28, 6695–6703. <https://doi.org/10.1002/adma.201600626>.
- Wang, Z., Shi, Z., Li, T., Chen, Y., Huang, W., 2016. Stability of perovskite solar cells: a prospective on the substitution of the a cation and X anion angewandte reviews, pp. 2–25. doi:10.1002/anie.201603694.
- Wang, R., Mujahid, M., Duan, Y., Wang, Z.K., Xue, J., Yang, Y., 2019. A Review of Perovskites Solar Cell Stability. *Adv. Funct. Mater.* <https://doi.org/10.1002/adfm.201808843>.
- Wang, F., Geng, W., Zhou, Y., Fang, H.-H., Tong, C.-J., Loi, M.A., et al., 2016. Phenylalkylamine passivation of organolead halide perovskites enabling high-efficiency and air-stable photovoltaic cells. *Adv. Mater.* 28, 9986–9992. <https://doi.org/10.1002/adma.201603062>.
- Wang, Q., Phung, N., Di Girolamo, D., Vivo, P., Abate, A., 2019. Enhancement in lifespan of halide perovskite solar cells. *Energy Environ. Sci.* 12, 865–886. <https://doi.org/10.1039/c8ee02852d>.
- Wang, D., Zheng, J., Wang, X., Gao, J., Kong, W., Cheng, C., et al., 2019. Improvement on the performance of perovskite solar cells by doctor-blade coating under ambient condition with hole-transporting material optimization. *J. Energy Chem.* 207–213. <https://doi.org/10.1016/j.jec.2019.03.023>.
- Wei, Z., Chen, H., Yan, K., Yang, S., 2014. Inkjet printing and instant chemical transformation of a CH₃NH₃PbI₃/nanocarbon electrode and interface for planar perovskite solar cells. *Angew. Chem. – Int. Ed.* 53, 13239–13243. <https://doi.org/10.1002/anie.201408638>.
- Wojciechowski, K., Leijtens, T., Siprova, S., Schlueter, C., Hörantner, M.T., Wang, J.T.-W.C., et al., 2015. 60 nm as an efficient n-type compact layer in perovskite solar cells. *J. Phys. Chem. Lett.* 6, 2399–2405. <https://doi.org/10.1021/acs.jpcllett.5b00902>.
- Wu, Y., Islam, A., Yang, X., Qin, C., Liu, J., Zhang, K., et al., 2014. Retarding the crystallization of PbI₂ for highly reproducible planar-structured perovskite solar cells via sequential deposition. *Energy Environ. Sci.* 7, 2934–2938. <https://doi.org/10.1039/c4ee01624f>.
- Xing, G., Mathews, N., Sun, S., Lim, S.S., Lam, Y.M., Gratzel, M., Mhaisalkar, S., Sum, T.C., 2013. Long-range balanced electron- and hole-transport lengths in organic-inorganic CH₃NH₃PbI₃. *Science* 342 (6156), 344–347. <https://doi.org/10.1126/science1243167>.
- Xiong, J., Yang, B., Cao, C., Wu, R., Huang, Y., Sun, J., et al., 2016. Interface degradation of perovskite solar cells and its modification using an annealing-free TiO₂NPs layer. *Org. Electron. Phys., Mater. Appl.* 30, 30–35. <https://doi.org/10.1016/j.orgel.2015.12.010>.
- Xu, L., Molaei Imenabadi, R., Vandenberghe, W.G., Hsu, J.W.P., 2018. Minimizing performance degradation induced by interfacial recombination in perovskite solar cells through tailoring of the transport layer electronic properties. *6. APL Mater.* <https://doi.org/10.1063/1.5021138>.
- Yang Z., Rajagopal A., Chueh C., Jo SB., Liu B., Zhao T., et al. Stable Low-Bandgap Pb – Sn Binary Perovskites for Tandem Solar Cells 2016. doi:10.1002/adma.201602696.
- Yang, S., Fu, W., Zhang, Z., Chen, H., Li, C.-Z., 2017. Recent advances in perovskite solar cells: efficiency, stability and lead-free perovskite. *J. Mater. Chem. A* 5, 11462–11482. <https://doi.org/10.1039/C7TA00366H>.
- Yang, W.S., Noh, J.H., Jeon, N.J., Kim, Y.C., Ryu, S., Seo, J., Seok, S.I., 2015. High-performance photovoltaic perovskite layers fabricated through intramolecular exchange. *Science* 348 (6240), 1234–1237. <https://doi.org/10.1126/scienceaaa9272>.
- Yang, Woon Seok, Park, Byung-Wook, Jung, Eui Hyuk, Jeon, Nam Joong, Kim, Young Chan, Lee, Dong Uk, Shin, Seong Sik, Seo, Gangwon, Kim, Eun Kyu, Noh, Jun Hong, Seok, Sang Il, 2017. Iodide management in formamidinium-lead-halide-based perovskite layers for efficient solar cells. *Science* (80–) 356, 1376–1379. <https://doi.org/10.1126/scienceaa2301>.
- Yang, Y., Peng, H., Liu, C., Arain, Z., Ding, Y., Ma, S., et al., 2019. Bi-functional additive engineering for high-performance perovskite solar cells with reduced trap density. *J. Mater. Chem. A* 7, 6450–6458. <https://doi.org/10.1039/c8ta11925b>.
- Yang, D., Yang, R., Wang, K., Wu, C., Zhu, X., Feng, J., et al., 2018. High efficiency planar-type perovskite solar cells with negligible hysteresis using EDTA-complexed SnO₂. *Nat. Commun.* 9. <https://doi.org/10.1038/s41467-018-05760-x>.
- Yang, Z., Zhang, S., Li, L., Chen, W., 2017. Research progress on large-area perovskite thin films and solar modules. *J. Mater.* 3, 231–244. <https://doi.org/10.1016/j.jmat.2017.09.002>.
- Yeo, J.S., Seo, Y.H., Jung, C.H., Na, S.I., 2019. Structural design considerations of solution-processable graphenes as interfacial materials: Via a controllable synthesis method for the achievement of highly efficient, stable, and printable planar perovskite solar cells. *Nanoscale* 11, 890–900. <https://doi.org/10.1039/c8nr05698f>.
- Yusoff, A.R.B.M., Nazeeruddin, M.K., 2016. Organohalide lead perovskites for photovoltaic applications. *J. Phys. Chem. Lett.* 7, 851–866. <https://doi.org/10.1021/acs.jpcllett.5b02893>.
- Zhang, C.-C., Wang, Z.-K., Li, M., Liu, Z.-Y., Yang, J.-E., Yang, Y.-G., et al., 2018. Electric-field assisted perovskite crystallization for high-performance solar cells. *J. Mater. Chem. A* 6, 1161–1170. <https://doi.org/10.1039/C7TA08204E>.
- Zhang, J., Zhang, T., Jiang, L., Bach, U., Cheng, Y.B., 2018. 4-tert-butylpyridine free hole transport materials for efficient perovskite solar cells: a new strategy to enhance the environmental and thermal stability. *ACS Energy Lett.* 3, 1677–1682. <https://doi.org/10.1021/acsenergylett.8b00786>.
- Zhang, Yupei, Laiquan, Haiquan, Su, Wei Huang, X.D., 2014. Materials chemistry A. *J. Mater. Chem. A*. <https://doi.org/10.1039/C4TA04996A>.
- Zhao, X., Kim, H.S., Seo, J.Y., Park, N.G., 2017. Effect of selective contacts on the thermal stability of perovskite solar cells. *ACS Appl. Mater. Interfaces* 9, 7148–7153. <https://doi.org/10.1021/acsami.6b13001>.

- doi.org/10.1021/acسامی.6b15673.
- Zheng, X., Chen, B., Dai, J., Fang, Y., Bai, Y., Lin, Y., et al., 2017. Using quaternary ammonium halide anions and cations, 17102, pp. 1–9, doi:10.1038/nenergy.2017.102.
- Zheng, L., Zhang, D., Ma, Y., Lu, Z., Chen, Z., Wang, S., et al., 2015. Morphology control of the perovskite films for efficient solar cells. *Dalt Trans.* 44, 10582–10593. <https://doi.org/10.1039/c4dt03869j>.
- Zhou, Y., Yin, X., Luo, Q., Zhao, X., Zhou, D., Han, J., Hao, F., Tai, M., Li, J., Liu, P., Jiang, K., Lin, H., 2018. Efficiently improving the stability of inverted perovskite solar cells by employing polyethylenimine-modified carbon nanotubes as electrodes. *ACS Appl. Mater. Interfaces* 10, 31384–31393. <https://doi.org/10.1021/acsami.8b10253>.
- Zhou, Y., Yang, M., Vasiliev, A.L., Garces, H.F., Zhao, Y., Wang, D., et al., 2015. Growth control of compact CH₃NH₃PbI₃ thin films via enhanced solid-state precursor reaction for efficient planar perovskite solar cells. *J. Mater. Chem. A* 3, 9249–9256. <https://doi.org/10.1039/C4TA07036D>.
- Zhou, Di, Zhou, Tiantian, Tian, Yu, Zhu, Xiaolong, Tu, Yafang, 2018. Perovskite-based solar cells: materials, methods, and future perspectives. *J. Nanomater.* 2018, 1–15. <https://doi.org/10.1155/2018/8148072>.
- Zhu, M., Hao, F., Ma, L., Bin, Song T., Miller, C.E., Wasielewski, M.R., et al., 2016. Solution-processed air-stable mesoscopic selenium solar cells. *ACS Energy Lett.* 1, 469–473. <https://doi.org/10.1021/acsenergylett.6b00249>.
- Zuo, F., Williams, S.T., Liang, P.W., Chueh, C.C., Liao, C.Y., Jen, A.K.Y., 2014. Binary-Metal Perovskites Toward High-Performance Planar-Heterojunction Hybrid Solar Cells. *Adv. Mater.* 26, 6454–6460. <https://doi.org/10.1002/adma.201401641>.